Geological Quarterly, 2008, **52** (4): 349–368

Ti remobilization and sulphide/sulphoarsenide mineralization in amphibolites: effect of granite intrusion (the Karkonosze–Izera Massif, SW Poland)

Ksenia MOCHNACKA, Teresa OBERC-DZIEDZIC, Wojciech MAYER and Adam PIECZKA

Mochnacka K., Oberc-Dziedzic T., Mayer W. and Pieczka A. (2008) — Ti remobilization and sulphide/sulphoarsenide mineralization in amphibolites: effect of granite intrusion (the Karkonosze–Izera Massif, SW Poland). Geol. Quart., **52** (4): 349–368. Warszawa.

Our studies focus on ore mineralization in a contact-metamorphic aureole, using the Variscan Karkonosze Granite pluton as an example. The Karkonosze intrusion is enveloped by an Early Palaeozoic (about 500 Ma) metamorphic complex of the Izera–Kowary Unit composed of a diverse assemblage of gneisses, granitic gneisses, schists, amphibolites and marbles. The Budniki ore mineralization site was discovered in the early 1950's at the SE margin of the pluton. The uneconomic Ti-oxide/silicate, Fe-Cu-Ni-Co-sulphide-sulphoarsenide, and uranium mineral deposits are hosted within amphibolites which were subjected to regional metamorphism followed by contact metamorphism. The Ti mineralization includes an ilmenite-titanite assemblage that originated from regional-metamorphic transformation of igneous Ti-bearing minerals, such as ilmenite and tschermakite, of the basic protoliths of amphibolites. During subsequent contact metamorphism, ilmenite was decomposed and, afterwards, Al-rich titanite and rutile were formed. The Ti remobilization was coeval with an early stage of superimposed Fe-Cu-Ni-Co-sulphide/sulphoarsenide mineralization (pyrrhotite, pyrite, pentlandite, arsenopyrite, chalcopyrite, sphalerite and Fe-Ni-Co-As-S phases), related to the activity of the Karkonosze Granite hydrothermal system. The ore minerals formed successively within a wide range of temperatures (625–250°C).

Ksenia Mochnacka, Wojciech Mayer, Adam Pieczka, Faculty of Geology, Geophysics and Environmental Protection, AGH-University of Science and Technology, Al. Mickiewicza 30, PL-30-059 Kraków, Poland; e-mail: kmoch@geol.agh.edu.pl; Teresa. Oberc-Dziedzic, Institute of Geological Sciences, University of Wrocław, Plac M. Borna 9, PL-50-204 Wrocław, Poland (received: February 04, 2008; accepted: August 28, 2008).

Key words: Karkonosze Granite, Ti mineralization, hydrothermal sulphide/sulphoarsenide mineralization, contact metamorphism.

INTRODUCTION

The southeastern part of the metamorphic cover of the Variscan Karkonosze Granite (Fig. 1) hosts diverse ore mineralization. One of the mineralization sites is the Budniki camp situated 3.5 km south-east of Karpacz, on the northern slope of the Kowary Range (Fig. 2). It is an abandoned exploration camp where uranium minerals were sought in the 1950's. This exploration activity left three adits and small waste dumps still accessible in a stream valley. These adits and dumps have yielded an interesting set of samples of amphibolites and quartzofeldspathic schists with Ti-Fe oxides and Fe, Cu, As, Co, Zn, Pb sulphides and sulphoarsenides. No uranium minerals have recently been detected.

The Budniki mineralization site was described briefly in an unpublished uranium exploration report (Kaczmarek, 1959). Based on that report and an other early data (Borucki *et al*., 1967), Mochnacka and Banaś (2000) classified the Budniki as "U-Th mineralization in nests spatially related to the Karkonosze Granite". However, no further detailed studies have been carried out.

The aim of this paper is to determine remobilization and mineralization processes triggered by contact metamorphism in a granite pluton aureole. We describe mutual relationships between the host rocks and the ore mineralization at the Budniki camp based on microscope studies of rock fabric, mineral intergrowths, supported by electron microprobe analyses of rock-forming and ore minerals. As a result, the metamorphic processes and related position of ore mineralization have been correlated. The formation of Ti-mineralization is interpreted in terms of metamorphic remobilization processes during contact metamorphism connected with the Karkonosze Granite intrusion, followed by sulphide and sulphosalt mineralization originating from the activity of hydrothermal solutions.

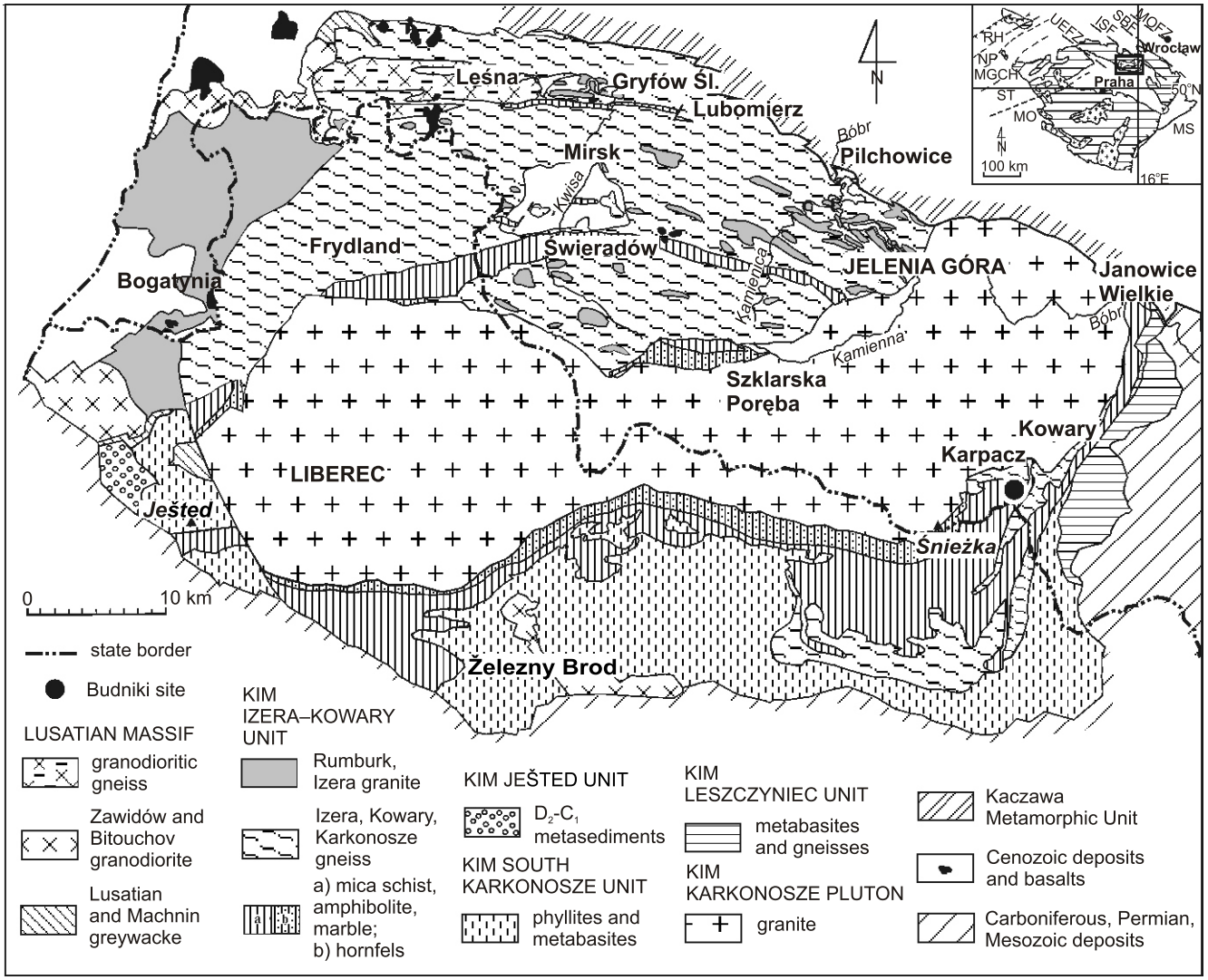

Fig. 1. Geological map of the Karkonosze–Izera Massif (compiled from Chaloupský, 1989; Mazur, 1995; Mazur and Aleksandrowski, 2001; Oberc-Dziedzic, 2003)

KIM — Karkonosze–Izera Massif; inset map: ISF — Intra-Sudetic Fault, MGCH — Mid-German Crystalline High, MO — Moldanubian Zone, MOFZ — Middle Odra Fault Zone, MS — Moravo-Silesian Zone, NP — Northern Phyllite Zone, RH — Rhenohercynian Zone, SBF — Sudetic Boundary Fault, ST — Saxothuringian Zone, UEFZ — Upper Elbe Fault Zone; rectangle shows the position of the KIM in the Bohemian Massif

MATERIALS AND METHODS

About 40 quartzofeldspathic schist and amphibolite samples were collected from the Budniki area for petrographic, mineralogical, geochemical and ore mineralization studies. Detailed microscope examinations were carried out on 20 thin sections under transmitted light and on 65 polished sections observed under reflected light.

The chemical composition of minerals was analyzed using the *CAMECA SX 100* microprobe analyzer at the Electron Microprobe Laboratory, University of Warsaw, operating at an acceleration voltage of 15 kV, a beam current of 10 nA for plagioclase and mica, and 20 nA for other minerals, a counting time of 20 s and a background time of 10 s. The raw data were corrected with the ZAF procedure contained in the *PAP* software provided by *CAMECA*.

GEOLOGICAL SETTING

The Karkonosze–Izera Massif (KIM; Fig. 1), situated in the Western Sudetes, includes the Karkonosze Granite pluton dated at 329 ±17 Ma using the Rb-Sr whole-rock method (Duthou *et al*., 1991) and its Neoproterozoic-Palaeozoic metamorphic envelope, which has been interpreted as a sequence of four distinct structural units: (l) the Izera–Kowary Unit, (2) the Ještěd Unit, (3) the South Karkonosze Unit and (4) the Leszczyniec Unit, showing different lithostratigraphies and metamorphic evolution (Mazur and Aleksandrowski, 2001). These units have been interpreted as elements of the nappe structure of the KIM formed in the Late Devonian and modified during the Early Carboniferous (*op. cit.*). The nappe pile was intruded by the Karkonosze Granite pluton. Its contact aureole is 600 to 2000 m wide (Mierzejewski and Oberc-Dziedzic, 1990).

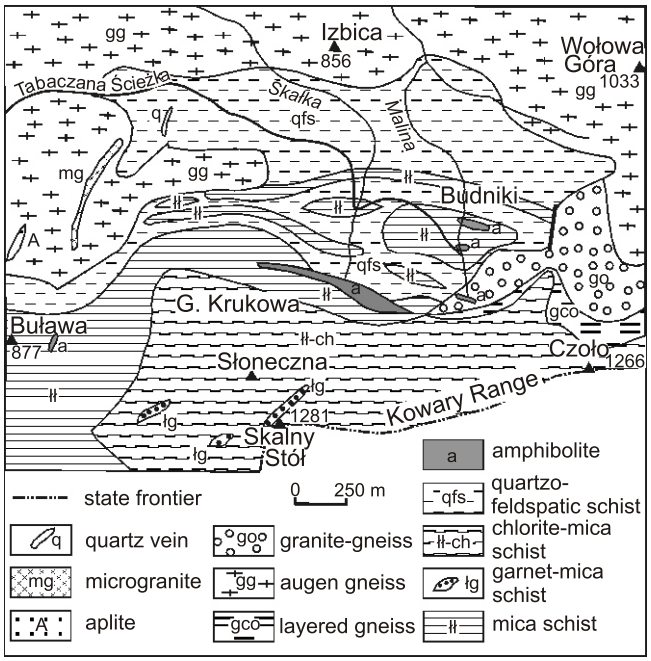

Fig. 2. Geological map of the Budniki site (after Różański, 1995)

The rocks studied belong to the southeastern part of the Izera–Kowary Unit (IKU) exposed between the southern margin of the Karkonosze pluton and the state border (Fig. 1). This part of the IKU (Fig. 2) includes the Kowary gneisses surrounded from the south by an assemblage of mica schists, quartzofeldspatic schists and amphibolites. The Budniki site is located in the northern part of this assemblage, about 1.5 km south of the margin of the Karkonosze Granite pluton, within the range of the contact-metasomatic aureole.

PETROGRAPHY

QUARTZOFELDSPATHIC SCHISTS

Quartzofeldspathic schists form small bodies (Fig. 2) within mica schists or 2–5 cm-thick intercalations in amphibolites. These are white-grey, very fine-grained rocks showing distinct foliation and lineation. The foliation is defined by flattened grains of quartz and albite, and rare, minute flakes of muscovite and biotite. Biotite occasionally also forms porphyroblasts, oblique to the foliation. Apatite is an accessory constituent, whereas grains of tourmaline are locally abundant. Rutile forms minute grains, some of which are arranged parallel to the foliation while others follow cross-cutting cracks. Such a position proves a relatively young age of the rutile.

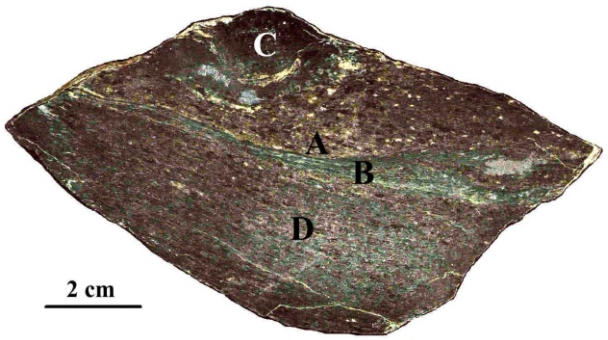

Fig. 3. Amphibolite sample B4 from the Budniki site

A, B, C, D — rock domains are described in the text

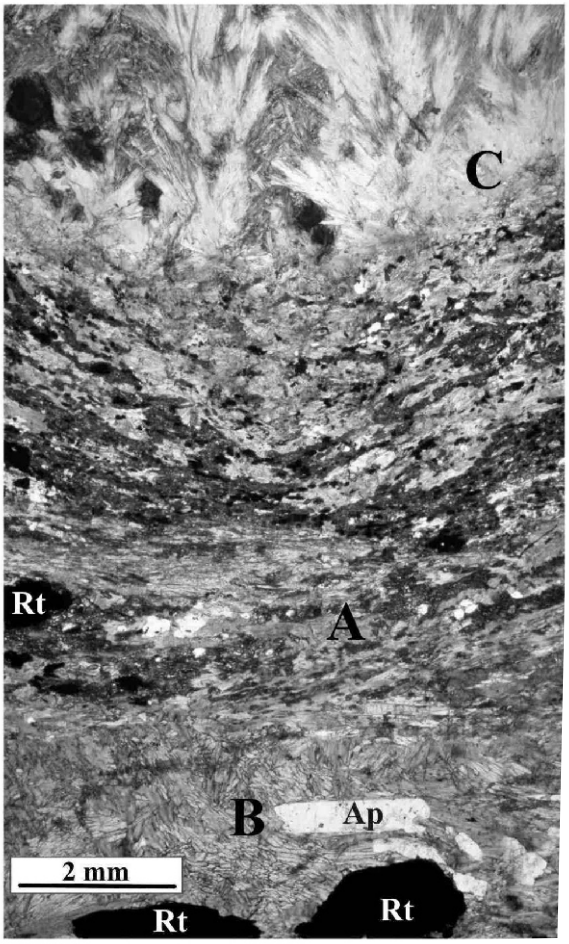

Fig. 4. Microscopic image of A, B, C domains from the amphibolite sample B4

Ap — apatite, Rt — rutile, crossed polars

AMPHIBOLITES

Amphibolites are dark green to blackish-green, fine-grained rocks, mostly of granoblastic texture. These can be subdivided into two varieties which differ in fabric and in the chemical compositions of the amphiboles and plagioclases. The first variety, represented by sample B2, is composed mainly of parallel, elongated grains of bluish-green hornblende and short packets of fine plagioclases, both defining the foliation. Strings of small, rounded or flattened ilmenite grains together with titanite and epidote follow the foliation. All minerals seem to be in equilibrium and show only weak signs of plagioclase and tschermakite decomposition.

The second variety of amphibolite, represented by sample B4 (Figs. 3 and 4), is composed of four types of domain. Do-

main A has greyish-green and dark green colours and shows a perfect foliation defined by flakes of biotite, strips of hornblende and layers of quartz and plagioclase. Long, blocky epidote grains and strings of ilmenite are parallel to the foliation. Domain B is composed of chaotically oriented, short, prismatic grains of amphiboles of magnesiohornblende and actinolite composition, and strips of older hornblende. It contains large crystals of rutile and apatite, and small grains of Ca-plagioclase and titanite. Domain C is represented by two ellipsoidal nodules, 2 cm and 0.5 cm long, with tails characteristic of porphyroclasts. The deflection of the matrix folia observed near the larger nodule may be interpreted as a result of local deformation around the pre-existing, rigid object (Vernon, 2004). The internal part of domain C is composed exclusively of radiating, acicular aggregates of actinolite. The needle-like actinolite crystals become thicker in the tails of the domain, which resembles a flower-like structure. The marginal part of domain C is composed of parallel grains of green or bluish-green amphibole, abundant ilmenite, the latter showing exsolution lamellae of rutile and replacements by titanite. Small patches comprising Na-plagioclase, epidote and titanite, together with apatite crystals, occur between amphibole grains and in the pressure shadows (tails). Domain D is composed of parallel-aligned, long epidote crystals, biotite flakes, small plagioclase grains and rare pyroxene.

The amphibolites also form small, 2 cm-thick, intercalations in a quartzofeldspathic schist composed of hornblende and, locally, of albite porphyroblasts.

The structural features and whole rock chemistry (not shown here) suggest that the rocks described reflect differentiation products of an original bimodal volcanic suite: basic lavas (the first variety of amphibolite), basic tuffs (the second variety of amphibolite), acidic tuffs (quartzofeldspathic schist) and intercalations of acidic and basic tuffs.

CHEMISTRY OF THE ROCK-FORMING MINERALS

The mineral chemistry was studied in two samples of amphibolite (B2, B4) and in one sample showing intercalations of amphibolite in quartzofeldspathic schist (B6). Systematic investigations were focused on plagioclases and amphiboles.

PLAGIOCLASE

In sample B2, representing the first variety of amphibolite, plagioclase varies from $An_{13.5}$ to $An_{25.5}$. The Or-admixture is low, between 0.3% and 1.3%, but sporadically can be as high as 8.2%. Some plagioclase grains show patches of albite ($Ab_{98–98.6}$ $An_{0.4–0.8}$ and $Or_{0.8–1.2}$) and K-feldspar, interpreted as a product of plagioclase decomposition during retrogression (Table 1).

In sample B4 (Fig. 4), representing the second variety of amphibolite, the An-contents in the plagioclase vary significantly on the scale of individual domains. In domain A, plagioclase grains show a compositional range of $An_{53.0}$–$An_{25.4}$ and contain 1.0–9.2% of Or-admixture. More Na-plagioclase grains ($An_{25.4}$) show patches (exsolutions) of K-feldspar, rich in Ab and An components (Or_{87}–$Ab_{5.3}$–$An_{7.6}$). Domain B, composed of chaotically oriented amphibole crystals, contains small grains of Ca-plagioclase ($An_{59.6–34.5}$). The marginal part of domain C, composed of green or bluish-green amphibole,

Table 1

Selected microprobe analyses of plagioclase from the Budniki amphibolite (in wt.%)

		B2			B4 domain A		B4 domain B	B4 domain C	B6	
SiO_2		61.34	68.26	64.51	60.28	54.02	52.87	66.51	64.54	69.43
Al_2O_3		24.12	19.55	21.83	25.1	28.6	29.57	20.72	22.59	19.73
CaO		5.29	0.17	2.85	5.23	11.11	12.23	1.44	3.62	0.15
FeO		0.18	0.07	0.21	0.15	0.00	0.23	0.28	0.07	0.04
BaO		0	0	0	0.01	0.02	0.05	0.45	–	–
Na_2O		8.42	11.51	9.96	7.42	5.27	4.54	10.73	9.31	11.66
K_2O		0.19	0.15	0.23	1.6	0.27	0.06	0.12	0.09	0.07
Total		99.55	99.69	99.58	99.79	99.29	99.53	99.8	100.23	101.07
Number of ions on the basis of 8 O										
Si		2.735	2.992	2.858	2.696	2.458	2.407	2.922	2.836	2.998
Al		1.268	1.01	1.14	1.323	1.534	1.586	1.073	1.17	1.004
Fe^{+2}		0.007	0.003	0.008	0.005	0,000	0.009	0.01	0.003	0.002
Ca		0.253	0.008	0.136	0.251	0.542	0.596	0.068	0.17	0.007
Ba		0.000	0.000	0.001	0	0	0.001	0.008	–	–
Na		0.728	0.978	0.855	0.644	0.465	0.4	0.914	0.794	0.976
K		0.012	0.009	0.014	0.091	0.016	0.003	0.007	0.005	0.004
Mol. %	or	1.1	0.8	1.3	9.2	1.5	0.3	0.7	0.5	0.4
	ab	73.4	98.4	85.2	65.3	45.4	40.0	91.7	81.9	99.0
	an	25.5	0.8	13.5	25.4	53.0	59.6	6.8	17.6	0.7

comprises Na-plagioclase ($An_{6.8–3.1}$) with Or varying between 0.7 and 1.4 Mol. % (Table 1).

In the amphibolite intercalation within the quartzofeldspathic schist (B6), plagioclase of $An_{17.6–0.7}$ composition forms small porphyroblasts.

AMPHIBOLE

Amphibole analyses are listed in Table 2. The nomenclature of the amphiboles studied was defined following the procedure described by Leake *et al*. (1997). Amphiboles from the Budniki site are members of the calcic group with $Ca_B>1.5$, $0.50<(Na+K)_A<0.50$ and $Ca_A<0.50$. These minerals belong to two generations that form separate grains. The younger amphiboles do not overgrow the older ones. The older generation is the main constituent in the first variety of amphibolite (B2 sample). It occurs also in the second variety (B4 sample) in B4 domain A and as relict strips within younger amphiboles in B4 domain B. The older amphibole is tschermakite with Mg/(Mg+Fe) ratios 0.57–0.61, or magnesiohornblende with Mg/(Mg+Fe) ratios of 0.62–0.78 (Fig. 5). Some tschermakite grains are patchily retrograded to magnesiohornblende. The old amphiboles show much higher contents of Al, Na, K and Ti, and lower contents of Ca than amphiboles of the new generation. Tschermakite is associated with plagioclase $An_{13.5}$ to $An_{25.5}$.

The younger generation of amphiboles occurs in the amphibolite intercalation in quartzofeldspathic schist (sample B6) and in the second variety of amphibolite (sample B4, Fig. 4) as: (1) chaotically oriented, short, prismatic grains (sample B6 and sample B4 domain B) or (2) radiating, acicular aggregates of sample B4 domain C (ellipsoidal nodules), and (3) parallel-arranged grains of green or bluish-green amphibole of the marginal part of domain C. The new, chaotically oriented amphiboles do not show compositional variations in single grains but reveal considerable variation as the entire group. In the Si-Mg/(Mg+Fe) diagram (Leake *et al*., 1997; Fig. 5) these minerals plot mainly into the field of magnesiohornblende, forming two groups separated by a distinct gap. Magnesiohornblende I forms a common array with the older generation of amphiboles. It has the same chemical characteristics as the magnesiohornlende member of the older amphiboles but shows a different structural position expressed by a chaotic orientation. It is associated with $An_{17.6-0.6}$ plagioclase. The magnesiohornblende II plots close to the adjacent parts of the actinolite and ferrohornblende fields (Fig. 5). Its composition differs from the composition of the magnesiohornblende I in its higher Si and lower Al contents. Magnesiohornblende II is associated with plagioclase of $An_{59.6}$–$An_{34.5}$ composition.

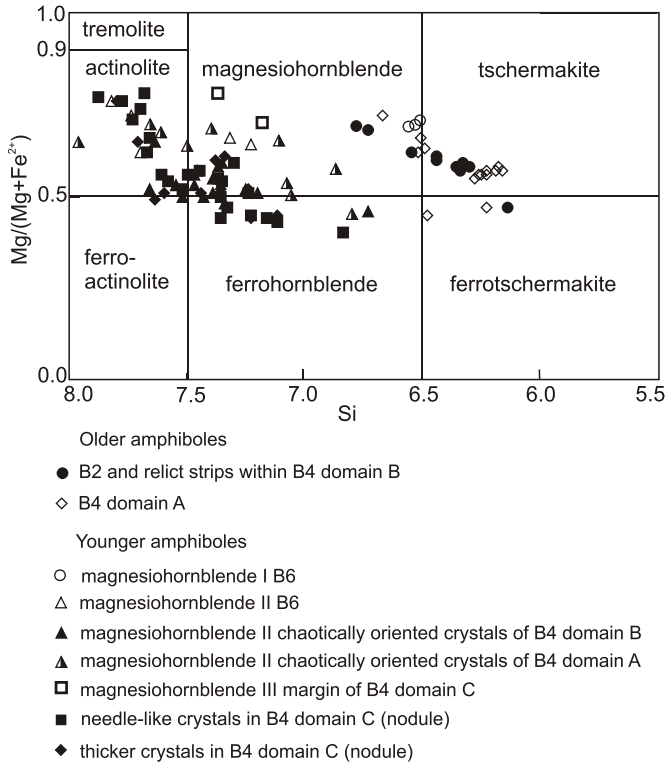

Fig. 5. Compositional variation of amphiboles from the Budniki amphibolites shown on the Leake *et al*. (1997) classification diagram; 97 analyses

Amphiboles forming the radiating and acicular aggregates in the nodules show compositional variations (Fig. 5). The oldest, central parts of radiating aggregates and the root parts of needle-like crystals are composed of actinolite low in Al and high in Mg. Towards the tailpieces of needles, the amphiboles changes from actinolite to magnesiohornblende and ferrohornblende in the outer parts of the needles and become similar in composition to the chaotically oriented grains. The composition of thicker amphibole crystals which form aggregates resembling flowers changes in a similar way as for needle-like crystals.

Parallel-arranged grains of amphibole from the marginal part of the C domain plot into the magnesiohornblende field. Their composition differs from the composition of the chaotic magnesiohornblende in having higher Mg and lower Fe contents (Fig. 5). Such differences composition, the position in the rocks and the association with albite, epidote and titanite allow definition of this variety of amphibole as magnesiohornblende III. It is associated with Na-plagioclase ($An_{6.8–3.1}$)

METAMORPHISM

The reconstruction of the metamorphic history of the Budniki rocks is difficult. The mineral assemblage of the quartzofeldspathic schists: quartz + albite + muscovite + biotite, which define the foliation, is not diagnostic of a specific P–T range. However, the presence of muscovite allowes use of the phengite geobarometer. Muscovite from the quartzofeldspathic schist shows a relatively low phengite content (Si^{4+}= 3.25 p.f.u. and Fe + Mg = 0.801). Thus, the calculated minimum pressure equal to 6 kb at 600°C (Massonne and Schreyer, 1987) took place during the formation of the foliation in the quartzofeldspathic schist.

Features of the amphibolite samples: (1) significant differences in chemical composition of the coexisting plagioclases and amphiboles, (2) replacement textures of Ti minerals, (3) new fabric imposed on earlier preserved-fabric, all point to a lack of metamorphic equilibrium. However, the fact that amphiboles and plagioclases

Selected microprobe analyses of amphibole

	B2 older amphibole				B4 domain B new amphibole			B4 domain C (nodule)				
								central part		thicker crystals		
SiO_2	45.85	42.44	42.56	43.9	50.83	51.14	50.3	52.84	54.63	49.95	49.51	46.9
TiO_2	0.41	0.49	0.45	0.4	0.12	0.15	0.2	0.03	0.04	0.12	0.2	0.17
Al_2O_3	10.14	13.11	12.75	11.64	3.71	3.33	4.52	2.42	1.49	5.24	4.61	6.29
Cr_2O_3	0.01	0.03	0.00	0.04	0.00	0.00	0.02	0.01	0.01	0	0	0
FeO	15.88	17.44	17.57	16.9	18.23	18.00	16.97	14.44	10.42	15.32	18.49	21.46
MnO	0.22	0.2	0.27	0.19	0.23	0.15	0.24	0.13	0.2	0.14	0.26	0.25
NiO	0.09	0.00	0.06	0.00	0.06	0.00	0.00	0	0	0.02	0.09	0
MgO	11.31	9.27	9.45	10.00	11.21	10.96	11.65	14.18	17.25	12.62	11.1	8.74
CaO	11.1	11.15	11.32	10.68	12.57	12.47	12.57	12.7	13.01	12.87	12.49	12.42
Na_2O	1.29	1.75	1.87	1.86	0.33	0.25	0.36	0.19	0.16	0.45	0.6	0.56
K_2O	0.32	0.52	0.48	0.43	0.21	0.19	0.24	0.09	0.05	0.21	0.34	0.5
Total	96.62	96.4	96.78	96.04	97.5	96.64	97.07	97.03	97.26	96.94	97.69	97.29
Si	6.734	6.351	6.36	6.549	7.553	7.656	7.468	7.713	7.802	7.38	7.365	7.12
Al^{IV}	1.266	1.649	1.64	1.451	0.447	0.344	0.532	0.287	0.198	0.62	0.635	0.88
Al^{VI}	0.49	0.664	0.607	0.596	0.203	0.244	0.259	0.129	0.053	0.292	0.173	0.245
Fe^{+3}	0.764	0.686	0.67	0.726	0.079	0.000	0.076	0.106	0.1	0.055	0.199	0.293
Cr	0.001	0.003	0.000	0.005	0.000	0.000	0.002	0.001	0.001	0.001	0.000	0.000
Ti	0.046	0.056	0.051	0.044	0.013	0.017	0.023	0.003	0.004	0.013	0.022	0.019
Mg	2.475	2.069	2.104	2.223	2.483	2.446	2.579	3.086	3.673	2.78	2.461	1.978
Fe	1.187	1.497	1.526	1.382	2.186	2.253	2.031	1.658	1.145	1.838	2.101	2.432
Mn	0.027	0.025	0.034	0.024	0.029	0.019	0.030	0.016	0.024	0.018	0.033	0.032
Ni	0.01	0.000	0.007	0.000	0.007	0.000	0.000	0.000	0.000	0.002	0.011	0.000
Ca	1.747	1.788	1.813	1.708	2.000	2.000	2.000	1.986	1.991	2.037	1.991	2.020
Na	0.367	0.509	0.542	0.538	0.095	0.072	0.103	0.054	0.044	0.129	0.173	0.165
K	0.059	0.1	0.092	0.082	0.040	0.037	0.046	0.017	0.009	0.04	0.065	0.097

c — central part of the grain, r — marginal part of the grain;
formulas of amphiboles calculated according to procedure of Robinson *et al*. (1982)

of specific compositions form pairs which are characteristic of particular types of domains suggests a local equilibrium and allows for a partial reconstruction of metamorphism conditions.

The Budniki amphibolites underwent metamorphic events recorded by four pairs of amphiboles and plagioclases showing different compositions:

1. tschermakite + plagioclase $An_{13.5}$ to $An_{25.5}$;
2. magnesiohornblende I + plagioclase $An_{\sim 15}$;
3. actinolite/magnesiohornblende II/ferrohornblende + Ca-plagioclase $An_{59.6–34.5}$;
4. magnesiohornblende III + Na-plagioclase $An_{6.8–3.1}$.

The temperatures of metamorphism which affected the amphibolites were estimated using the amphibole-plagioclase geothermometer for silica-saturated and silica-undersaturated rocks (thermometer B; Holland and Blundy, 1994) and compared with results derived from the graphical geothermobarometer of Plyusnina (1982) based on the Al-content of amphibole and Ca-content of plagioclase.

As the Budniki amphibolite does not contain critical minerals such as garnet or orthoamphibole, many popular geobarometers for metamorphic rocks cannot be used for pressure estimation. Similarly, the geobarometers based on the Al-content in hornblende cannot be applied for amphibolites because they are recommended for magmatic rocks. An exception among these geobarometers is the graphical geothermobarometer of Plyusnina (1982) based on the Al-content of amphibole and the Ca-content of plagioclase, and calibrated for metabasites metamorphosed under epidote-amphibolite- and amphibolite-facies conditions. We used this, although it often yielded unrealistic values of temperature and pressure. The pressure conditions were also estimated, on the basis of the mineral assemblages in the hornfelses surrounding the amphibolite, as not higher than 2–3 kbar (Mochnacka *et al*., 2007). Such pressure was assumed in the calculation of temperature for the second, third and fourth plagioclase-amphibole pairs.

The first amphibole-plagioclase pair defines the foliation and refers to the regional stage of metamorphism. At a pressure of 6 kbar (the value estimated for the quartzofeldspathic schist accompanying the amphibolite) the temperatures calculated with the Holland and Blundy geothermometer (1994) were 675°C for the pair tschermakite + plagioclase $An_{25.5}$ and 650°C for the pair tschermakite + plagioclase $An_{16.2}$. The graphical geothermobarometer of Plyusnina (1982) yielded much lower temperatures: 530°C and 510°C, respectively, and a pressure of

Table 2

from the Budniki amphibolite (in wt.%)

B4 domain C (nodule)				B6				B4 a	
needle crystal		marginal part							
55.22	52.63	49.28	50.99	49.79	50.29	45.02	45.17	47.39	48.78
0.02	0.02	0.22	0.07	0.16	0.18	0.41	0.34	0.17	0.17
1.22	2.82	6.23	4.04	6.14	5.4	12.19	13.13	7.17	7.14
0.02	0.01	0.01	0.05	0	0	0	0.06	0	0.02
9.59	14.18	14.21	14.27	15.73	14.62	14.94	15.64	19.66	15.14
0.13	0.19	0.18	0.17	0.23	0.21	0.2	0.24	0.25	0.32
0	0	0.05	0.00	0.04	0.04	0	0	0.09	0
17.56	14.31	13.7	14.81	12.68	13.45	11.55	10.74	9.75	12.68
13.14	12.79	12.3	11.73	12.44	12.58	11.09	10.41	12.51	12.53
0.13	0.27	0.66	0.26	0.68	0.62	1.84	1.65	0.61	0.87
0.05	0.12	0.14	0.09	0.12	0.11	0.21	0.26	0.44	0.11
97.08	97.34	96.98	96.48	98.01	97.5	97.45	97.64	98.04	97.76
7.879	7.659	7.175	7.366	7.238	7.323	6.534	6.507	7.062	7.112
0.121	0.341	0.825	0.634	0.762	0.677	1.466	1.493	0.938	0.888
0.084	0.143	0.244	0.053	0.29	0.25	0.619	0.736	0.321	0.339
0.000	0.105	0.482	0.839	0.349	0.267	0.753	0.954	0.322	0.33
0.001	0.001	0.001	0.005	0	0	0	0.007	0	0.002
0.003	0.002	0.024	0.008	0.017	0.02	0.045	0.037	0.019	0.018
3.735	3.105	2.973	3.189	2.748	2.92	2.499	2.306	2.165	2.756
1.145	1.621	1.249	0.885	1.563	1.513	1.061	0.931	2.129	1.516
0.016	0.023	0.021	0.021	0.028	0.026	0.025	0.029	0.032	0.039
0.000	0.000	0.006	0.000	0.005	0.005	0	0	0.011	0
2.009	1.994	1.918	1.816	1.938	1.963	1.724	1.607	1.998	1.957
0.036	0.076	0.187	0.073	0.192	0.175	0.518	0.461	0.176	0.247
0.009	0.022	0.026	0.016	0.022	0.02	0.039	0.048	0.084	0.02

6.3–8 kbar, comparable with the value of pressure estimated for the quartzofeldspathic schists.

The temperatures calculated for the first amphibole-plagioclase pair using Holland and Blundy (1994) geothermometer seem to be too high. The range of temperatures during the first stage of metamorphism is confined by the absence of clinopyroxene which should appear around 650°C and the presence of small amount of epidote which is not typically found in amphibolites that were metamorphosed at temperatures higher than 600°C (Bucher and Frey, 1994). The absence of clinopyroxene and the presence of epidote indicate maximum peak-metamorphic conditions of about 600°C. On the contrary, the results — 530°C and 510°C — of the graphical geothermobarometer after Plyusnina (1982) seem to be too low. In such temperatures, plagioclase and amphibole should have different chemical compositions than the first pair of hornblende and plagioclase, and chlorite should be present. The absence of chlorite suggests that the minimum temperature was about 550°C, because this mineral completely disappears at this temperature.

Over 100°C discrepancies between the two geothermometers used corroborate opinions (Nasir and Okrusch, 1997; John *et al*., 1999) that the plagioclase-hornblende thermometers yield either too low (Plyushnina, 1982) or too high temperatures (Holland and Blundy, 1994).

The second pair: magnesiohornblende I + plagioclase $An_{\sim 15}$ was found in the amphibolite intercalation in quartzofeldspathic schist (sample B6). The chaotic orientation of both minerals indicates crystallization without stress. The temperature calculated with the Holland and Blundy geothermometer (Holland and Blundy, 1994) for the second pair was about 540°C, at the assumed pressure of 2 kbar and 510°C and 2 kbar using the graphical geothermobarometer of Plyusnina (1982).

In sample B4, some older amphiboles in strips preserved within younger, chaotic amphiboles show the same composition as magnesiohornblende I and magnesiohornblende patches in the tschermakite. This observation suggests that the retrogression of the tschermakite took place under similar P–T conditions as the crystallization of magnesiohornblende I.

The third pair — chaotically oriented actinolite/magnesiohornblende II/ferrohornblende and Ca-plagioclase $An_{59.6–34.5}$ — was found in several domains. As in the second pair, the lack of preferred orientation of amphiboles suggests crystallization without stress. The crystallization temperature

of the third pair was estimated at 622–635°C at the assumed pressure of 2 kbar (Holland and Blundy, 1994). This estimation seems to be realistic and is supported by the appearance of clinopyroxene in the same association. In the Plyusnina (1982) diagram, analyses of the third pair are situated outside the boundary conditions of this geothermobarometer.

The fourth pair: magnesiohornblende III + Na-plagioclase $An_{6.8–3.1}$ occurs in the marginal part of the amphibole nodule. The estimated temperature is 473–511°C at the assumed pressure of 2 kbar (Holland and Blundy, 1994). A similar result was obtained using the Plyushnina (1982) geothermobarometer.

The calculated temperatures, together with the observed succession of minerals and fabrics, allow the sequence of metamorphic events in the Budniki area to be determined. We interpret these as two discrete metamorphic events, with older regional metamorphism and younger contact metamorphism, the latter connected with the Karkonosze Granite intrusion. During the first event, i.e. the Variscan regional metamorphism, the products of Early Palaeozic (Oberc-Dziedzic *et al*., in press) bimodal volcanism were metamorphosed and deformed under amphibolite facies conditions, within temperatures range estimated from the first amphibole-plagioclase pair (600–550°C). The signs of plagioclase and tschermakite decomposition suggest a subsequent decrease in temperature, still during that regional metamorphic event.

The contact metamorphism connected with the Karkonosze intrusion caused remarkable but unevenly distributed changes in mineral composition, mineral associations and rock textures, leaving some parts of amphibolites untouched and others completely transformed. Such heterogeneity of change indicates that the degree of metamorphism was caused not only by temperature but also by magmatic fluids. The migration of fluids was facilitated by structural and compositional discontinuities such as foliation and layering. During the contact metamorphism, the rocks were subjected to changing temperatures, as suggested by the calculations for the 2nd, 3rd and 4th pairs of amphibole and plagioclase. The first episode of contact metamorphism took place at about 540°C, i.e. at temperature lower than those of the regional metamorphism. It caused retrograded reactions in the existing tschermakite and plagioclase $An_{13.5}$ to $An_{25.5}$ in some places, and crystallization of the new amphibole and plagioclase (magnesiohornblende I + plagioclase $An_{\sim 15}$) having similar chemical compositions as the retrograded patches in tschermakite and plagioclase $An_{25.5}$. In the course of the next episode, the temperature gradually increased, as recorded by the changes of amphibole composition from actinolite to magnesiohornblende and ferrohornblende in the nodules. The peak temperature of 622–635°C during that episode is reflected by the coexistence of chaotic magnesiohornblende II and Ca-plagioclase grains, and by the appearance of clinopyroxene. The actinolite + Ca-plagioclase assemblage is relatively common in metabasites from contact aureoles and usually occurs immediately on the low-temperature side of the amphibolite facies zone (Miyashiro, 1994). Our calculations show that the magnesiohornblende II + Ca-plagioclase assemblage, typical of the Budniki amphibolites, crystallized at higher temperatures.

The actinolite/magnesio-/ferrohornblende nodule shows a porphyroclast-like shape. This feature, together with the parallel arrangement of amphiboles surrounding the nodule, are evidence of shearing after the formation of the nodule. The shearing took place at temperatures of 473–511°C calculated from the fourth amphibole + plagioclase pair. The rocks were again subjected to retrogression, which caused decomposition of Ca-plagioclase into albite and epidote. The amphibole + albite + epidote assemblage is characteristic of the late phase of contact metamorphism.

TI MINERALIZATION

In the Budniki quartzofeldspathic schist, the total content of TiO_2 is 0.545 wt.% (Oberc-Dziedzic *et al*., in press). Ti mineralization is represented by rutile. It occurs as single, minute grains, arranged parallel to the foliation or scattered along cracks. Rutile grains occur also near muscovite and chlorite, both replacing biotite (Fig. 6A). The textural position of rutile indicates crystallization after brittle deformation and is probably connected with hydrothermal fluids circulating along the foliation planes and cracks. It does not necessarily mean that Ti was supplied from an external source, but it might have been present in the protolith of the quartzofeldspathic schist. However, biotite should be excluded as the main source of Ti because of its scarcity in the quartzofeldspathic schist.

The Budniki amphibolites contain much more TiO_2 (4.398 wt.%) than the quartzofeldspathic schist (Oberc-Dziedzic *et al*., in press). Ti-minerals are represented by ilmenite, rutile and titanite. The relationships between these minerals, their sequence and their position in the rock domains highlight the development of Ti mineralization and help to define more precisely the metamorphic conditions.

In the first variety of amphibolite (B2), Ti minerals are represented by clusters or aggregates of ilmenite and titanite which parallel the foliation (Fig. 6B); in places these are accompanied by minute grains of chalcopyrite (Fig. 6C). Initially, these two Ti-phases were apparently in equilibrium (Fig. 6C) as they do not exhibit any reaction or texture alteration. The mutual inclusions: ilmenite in titanite and titanite in ilmenite are probably an effect of the section or indicate some retrogression. The structural position of ilmenite and titanite suggests that their crystallization was coeval with the deformation which produced the foliation defined by tschermakite and plagioclase $An_{13.5}$ to $An_{25.5}$.

Some ilmenite grains show intergrowths with rutile. Such grains were found in the amphibolite intercalation in quartzofeldspathic schists (sample B6, Fig. 6D, E) where these minerals form inclusions in the plagioclase that defines the foliation. Ilmenite intergrowths with rutile also occur in the matrix of the external part of the actinolite nodule in sample B4 (Fig. 6F). In both cases the position of ilmenite-rutile intergrowths suggests that their origin is related to shearing along the foliation.

In the second variety of amphibolite (sample B4) the relationships between Ti minerals are more complicated. Generally, ilmenite is replaced by titanite (Fig. 6F, G). This process usually begins at the margins of ilmenite crystals and gradually proceeds into the interiors, leaving small patches of ilmenite inside the titanite (Fig. 6G). The titanite rims around ilmenite,

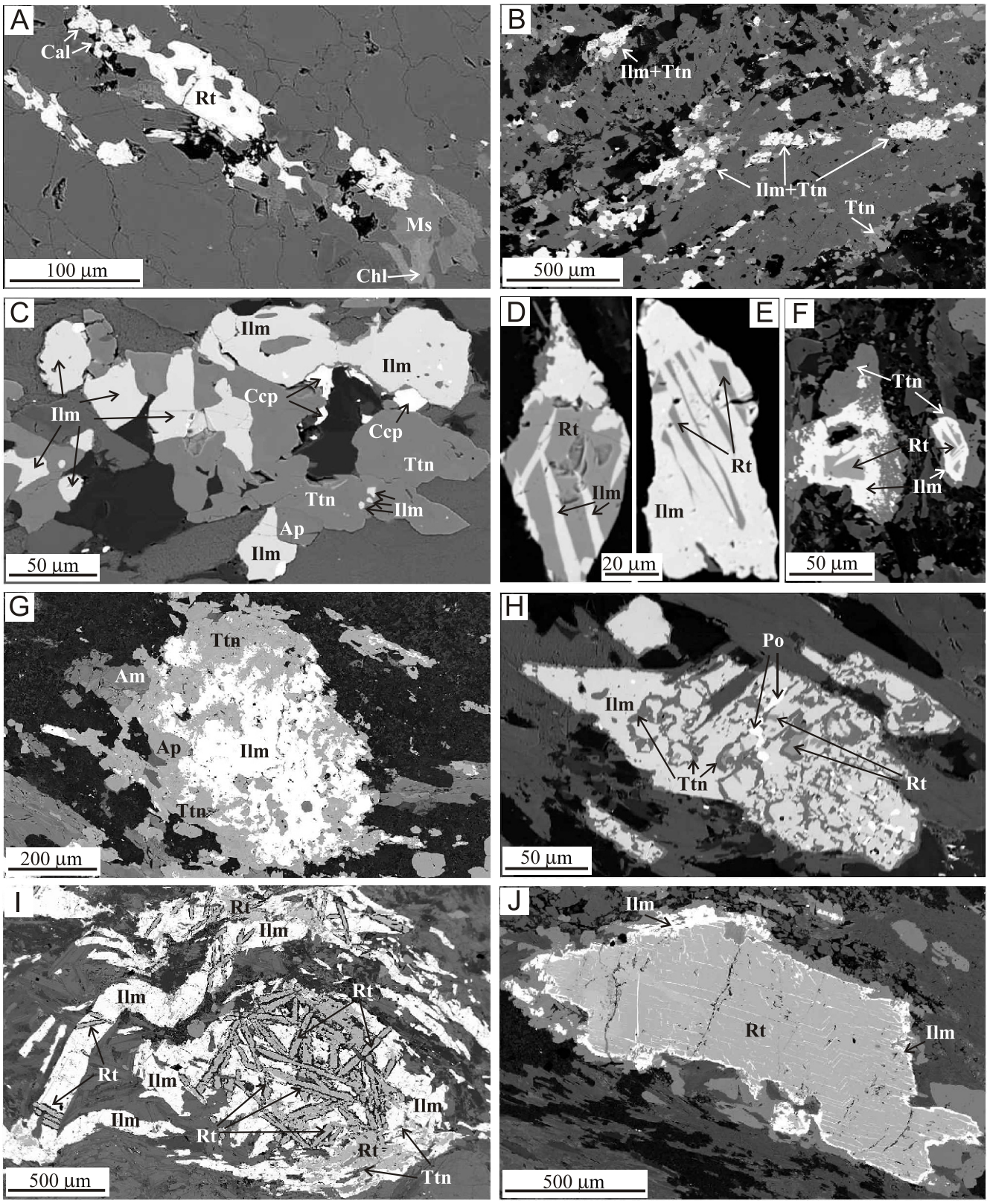

Fig. 6. BSE images of Ti minerals from the Budniki site

Quartzofeldspathic schist: **A** — rutile grains associated with calcite, muscovite and chlorite replacing biotite; sample B3; amphibolite: **B** — aggregates of ilmenite and titanite arranged parallel to the foliation in amphibolite; sample B2; **C** — ilmenite and titanite associated with minute grains of chalcopyrite; sample B2; **D**, **E** — rutile-ilmenite intergrowths showing different proportions of Ilm and Rt; amphibolite intercalation in quartzofeldspathic schist, sample B6; **F** — rutile-ilmenite intergrowths surrounded by titanite; sample B4; **G** — ilmenite patchily replaced by titanite; sample B4; **H** — ilmenite grain elongated concordantly with foliation, patchily replaced by rutile rimmed by titanite and intergrown by pyrrhotite, sample Bud-7; **I** — pseudomorph after ilmenite composed of rutile needles forming a trigonal network; minute patches of titanite occur in the external part of the pseudomorph; sample Bud-Z; **J** — large rutile grain having ilmenite exsolutions along network of cleavage planes and altered to ilmenite at the margins; sample B4; abbreviations: Am — amphibole, Ap — apatite, Cal — calcite, Ccp — chalcopyrite, Chl — chlorite, Ilm — ilmenite, Ms — muscovite, Po — pyrrhotite, Py — pyrite, Rt — rutile, Ttn — titanite

Table 3

Average chemical composition and formulae of Ti minerals from the Budniki amphibolite analyzed using an electron microprobe (in wt.%)

	Rutile					Ilmenite	A-1	Titanite				
	I	II	III	IV	V			1	2	3	4	5
SiO_2	0.00	0.00	0.00	0.00	0.00	0.00	30.47	29.96	30.44	30.46	30.24	30.44
Ta_2O5	0.16	0.08	0.02	0.00	0.01	0.04	–	0.19	0.21	0.20	0.19	0.00
FeO	1.94	1.00	0.75	0.46	0.29	45.21	0.41	0.70	0.65	0.74	0.56	1.24
MnO	0.00	0.00	0.00	0.00	0.00	1.83	0.09	0.04	0.00	0.00	0.03	0.02
TiO_2	92.69	96.30	96.83	98.42	98.46	51.80	38.63	34.36	35.27	36.90	37.24	35.13
SnO_2	0.04	0.02	0.04	0.01	0.02	0.00	–	2.20	0.44	0.21	0.00	0.00
ZrO_2	0.00	0.00	0.00	0.00	0.00	0.00	–	0.00	0.00	0.00	0.00	0.00
Nb_2O_5	3.25	1.73	0.57	0.25	0.05	0.04	–	0.08	0.02	0.00	0.00	0.00
ThO_2	0.00	0.00	0.00	0.00	0.00	0.00	–	0.00	0.00	0.00	0.00	0.00
UO_2	0.00	0.00	0.00	0.00	0.00	0.00	–	0.00	0.00	0.00	0.00	0.00
CaO	0.00	0.00	0.00	0.00	0.00	0.00	28.89	27.32	28.00	27.70	28.42	28.59
WO_3	1.09	0.27	0.84	0.04	0.01	0.00	–	0.00	0.00	0.00	0.00	0.00
Al_2O_3	0.00	0.00	0.00	0.00	0.00	0.00	1.11	2.36	2.88	1.87	1.71	2.45
V_2O_3	0.85	0.76	0.80	0.62	0.76	0.36	0.22	0.16	0.19	0.15	0.11	0.05
H_2O	–	–	–	–	–	–	–	0.18	0.24	0.14	0.21	0.39
Total	100.01	100.15	99.46	99.81	99.60	99.28	99.85	97.56	98.34	98.37	98.72	98.32
Number of ions on: 2 O (rutile), 3 O (ilmenite), 4 O (titanite)												
Si	0.000	0.000	0.000	0.000	0.000	0.000	–	1.005	1.002	1.006	0.994	0.999
Ta	0.001	0.000	0.000	0.000	0.000	0.000	–	0.002	0.002	0.002	0.002	0.000
Fe	0.022	0.010	0.008	0.005	0.003	0.963	–	0.019	0.018	0.020	0.015	0.034
Mn	0.000	0.000	0.000	0.000	0.000	0.040	–	0.001	0.000	0.000	0.001	0.001
Ti	0.950	0.971	0.979	0.989	0.992	0.992	–	0.867	0.873	0.917	0.921	0.867
Sn	0.000	0.000	0.000	0.000	0.000	0.000	–	0.029	0.006	0.003	0.000	0.000
Zr	0.000	0.000	0.000	0.000	0.000	0.000	–	0.000	0.000	0.000	0.000	0.000
Nb	0.020	0.010	0.003	0.002	0.000	0.001	–	0.001	0.000	0.000	0.000	0.000
Th	0.000	0.000	0.000	0.000	0.000	0.000	–	0.000	0.000	0.000	0.000	0.000
U	0.000	0.000	0.000	0.000	0.000	0.000	–	0.000	0.000	0.000	0.000	0.000
Ca	0.000	0.000	0.000	0.000	0.000	0.000	–	0.982	0.987	0.980	1.001	1.005
W	0.004	0.001	0.003	0.000	0.000	0.000	–	0.000	0.000	0.000	0.000	0.000
Al	0.000	0.000	0.000	0.000	0.000	0.000	–	0.093	0.112	0.073	0.066	0.095
V	0.009	0.008	0.009	0.007	0.008	0.007	–	0.004	0.005	0.004	0.003	0.001
OH^-	–	–	–	–	–		–	0.041	0.052	0.030	0.045	0.085
Total	1.006	1.001	1.002	1.002	1.004	2.003						

intergrown with rutile (Fig. 6F) indicate that the replacement of ilmenite by titanite took place after the deformation and it affected only grains in the matrix (Fig. 6F) which were not protected by the host plagioclase (Fig. 6D, E).

Occasionally, ilmenite is replaced by rutile (Fig. 6H, I). The replacement leads to the formation of rutile patches rimmed by titanite (Fig. 6H). Small inclusions of chalcopyrite and pyrrhotite suggest that such replacement might have been caused by hydrothermal processes and might have used Fe released from ilmenite (Ramdohr, 1969). Another pattern of replacement leads to the appearance of rutile pseudomorphs after ilmenite composed of rutile needles forming a trigonal network (Fig. 6I). The pseudomorphs have the shape of δ-type porphyroclasts and are associated with long, asymmetrically folded crystals of ilmenite. The rotation of pseudomorphs took place after the replacement and was coeval with the deformation of the amphibole nodule.

The next generation of Ti minerals is rutile associated with new, chaotic magnesiohornblende II and large apatite crystals. This rutile reaches up to several millimetres in size and tends to host numerous ilmenite exsolutions along cleavage planes and, locally, reveals distinct alteration into ilmenite at the margins (Fig. 6J).

The chemical composition of Ti minerals is given in Table 3. The large rutile grains show variable composition with irregular zones enriched in Nb_2O_5 (up to 3.25 wt.%), FeO (up to 1.94 wt.%), WO_3 (up to 1.09 wt.%) and traces of Ta_2O_5 (Table 3, analysis I), surrounded by zones with distinctly lower contents of these components (Table 3, analyses II, III). The rutile needles in pseudomorphs after ilmenite usually contain only traces of Fe and Nb, sometimes also W (Table 3, analyses IV, V) whereas vanadium is a common component (0.6–0.8 wt.%).

By contrast, the ilmenite is highly homogeneous. Smaller grains of ilmenite dispersed within amphibolite often show

high enrichment in Mn, with a mean MnO content of about 4.5 wt.% (not shown in Table 3). Both the ilmenite forming the lamellar exsolutions within large rutile grains and overgrowing them, as well as the ilmenite forming asymmetrically folded crystals, are slightly less enriched in Mn, with a mean MnO content of 1.83 wt.% (Table 3). Besides Mn, only V_2O_3 is a significant component (0.36 wt.%).

The chemical composition of the titanite is also variable. In the first-type amphibolite (B2), titanite which is in equilibrium with ilmenite contains 1.11 wt.% Al_2O_3 (Table 3, analysis A-1). In the second variety of amphibolite (B4), all analyzed crystals of titanite replacing ilmenite are enriched in Al compared with the first variety. They contain 1.8 to almost 2.9 wt.% Al_2O_3 (Table 3, analyses 1–5), and sporadically, up to 4.5 wt.%. The V_2O_3 content is low, usually 0.1–0.2 wt.%. Titanite crystals with significant amounts of Sn (up to 2.2 wt.% SnO_2) were only occasionally observed.

The processes of mutual replacement of Ti minerals probably started at the end of the regional metamorphic event and became very intense during the contact metamorphism. The replacement processes were controlled by temperature, fluids, local mineral assemblages (chemical composition) and rock structures.

The replacement of ilmenite by titanite was connected with retrogression at the end of the regional metamorphic event and/or at the beginning of the contact metamorphism, as well as during the late phase of the latter. The retrogression was enhanced by the presence of fluids and it caused the decomposition of plagioclases and the release of Ca and Al, facilitating the formation of titanite enriched in Al. Harlov *et al*. (2006) showed that the formation of Al-bearing titanite during amphibolite and greenschists facies metamorphism depends not only on P, T, bulk-rock composition and composition of the coexisting fluids but also on fO_2 and fH_2O.

The replacement of ilmenite by rutile is only occasionally observed. It might have occurred at the same time as the replacement of ilmenite by titanite and might have been confined to the domains of rock devoid of Ca — the necessary component in the formation of titanite. However, it is also possible that the replacement of ilmenite by rutile took place a little later than the replacement of ilmenite by titanite and occurred during the crystallization of the actinolite/magnesiohornblende II + Ca-plagioclase assemblage, which consumed all the available Ca. The changes of chemical composition of amphiboles in the nodules point to a continuous increase of Fe content during crystallization of the actinolite–magnesiohornblende II–ferrohornblende array. The amphiboles of this array contain also considerably less Ti than tschermakite, which was an original constituent of the rocks and became unstable under new conditions. A simultaneous decrease of Fe and Ca ions, especially in domains composed of new, chaotic magnesiohornblende II, resulted in the crystallization of large grains of rutile which were subsequently imperceptibly altered to ilmenite along the cleavage planes and grain margins.

The later retrogression was responsible for the crystallization of magnesiohornblende III + albite + epidote + titanite assemblage. It also provided conditions for a continuation of the replacement of ilmenite by titanite.

SULPHIDE/SULPHOARSENIDE MINERALIZATION

Microscopy observations revealed the presence of a diversified assemblage of ore minerals. Besides Ti phases and enclosed, tiny inclusions of scheelite and wolframite, the ore assemblage is composed mainly of pyrrhotite, pyrite, chalcopyrite, sphalerite and arsenopyrite. Other phases, such as cobaltite, gersdorffite, marcasite, galena and pentlandite, occur only occasionally.

The ore minerals form disseminated, spotty, streaky and veinlet structures within various types of amphibolites. Because the samples were collected exclusively from dumps, it is impossible to evaluate the relationships between the various ore structures.

PYRRHOTITE

Pyrrhotite forms disseminated and spotted structures. Some grains are arranged concordantly with the amphibolite foliation, while other, larger, isometric or elongated aggregates are commonly intergrown with gangue minerals (Fig 7A). Pyrrhotite forms intergrowths with chalcopyrite. Both phases seem to be contemporaneous (Fig 7B). Pyrrhotite crystals are commonly replaced by marcasite which rims its grains and grows inside, along cleavage planes (Fig 7C).

The chemical composition of pyrrhotite is generally uniform. Grains hosting exsolutions of pentlandite are highest in Ni (mean value about 1.10 wt.%; Table 4), whereas in the remaining grains Ni contents range typically from 0.40 to 0.80 wt.%. In contrast, Co does not concentrate in pyrrhotite as its mean content never exceeds 0.1 wt.% (Table 4).

PYRITE

Pyrite forms fine, disseminated crystals, intergrowths with pyrrhotite (Fig. 7C), aggregates of hipidiomorphic crystals arranged parallel to the foliation (Fig. 8B) and intergrowths with chalcopyrite.

CHALCOPYRITE

Chalcopyrite occurs as single, disseminated, xenomorphic grains or intergrowths with pyrrhotite (Fig. 7B), arsenopyrite (Fig. 7D), marcasite (Fig. 8A) and sphalerite (Fig. 8D). Common also are tiny exsolutions in sphalerite.

The typical composition of chalcopyrite is almost stoichiometric (Table 5, Chalcopyrite I) but exsolutions in sphalerite show a mean content of 0.87 ±0.40 wt.% Zn (sometimes up to 2.64 wt.%; Table 5, Chalcopyrite II and III).

SPHALERITE

Sphalerite occurs as single crystals, aggregates of xenomorphic grains and intergrowths with marcasite (Figs. 7E and 8A, C), galena (Fig. 8C) and chalcopyrite (Fig. 8D). Commonly, sphalerite aggregates reveal the presence of fine, oval exsolutions of chalcopyrite.

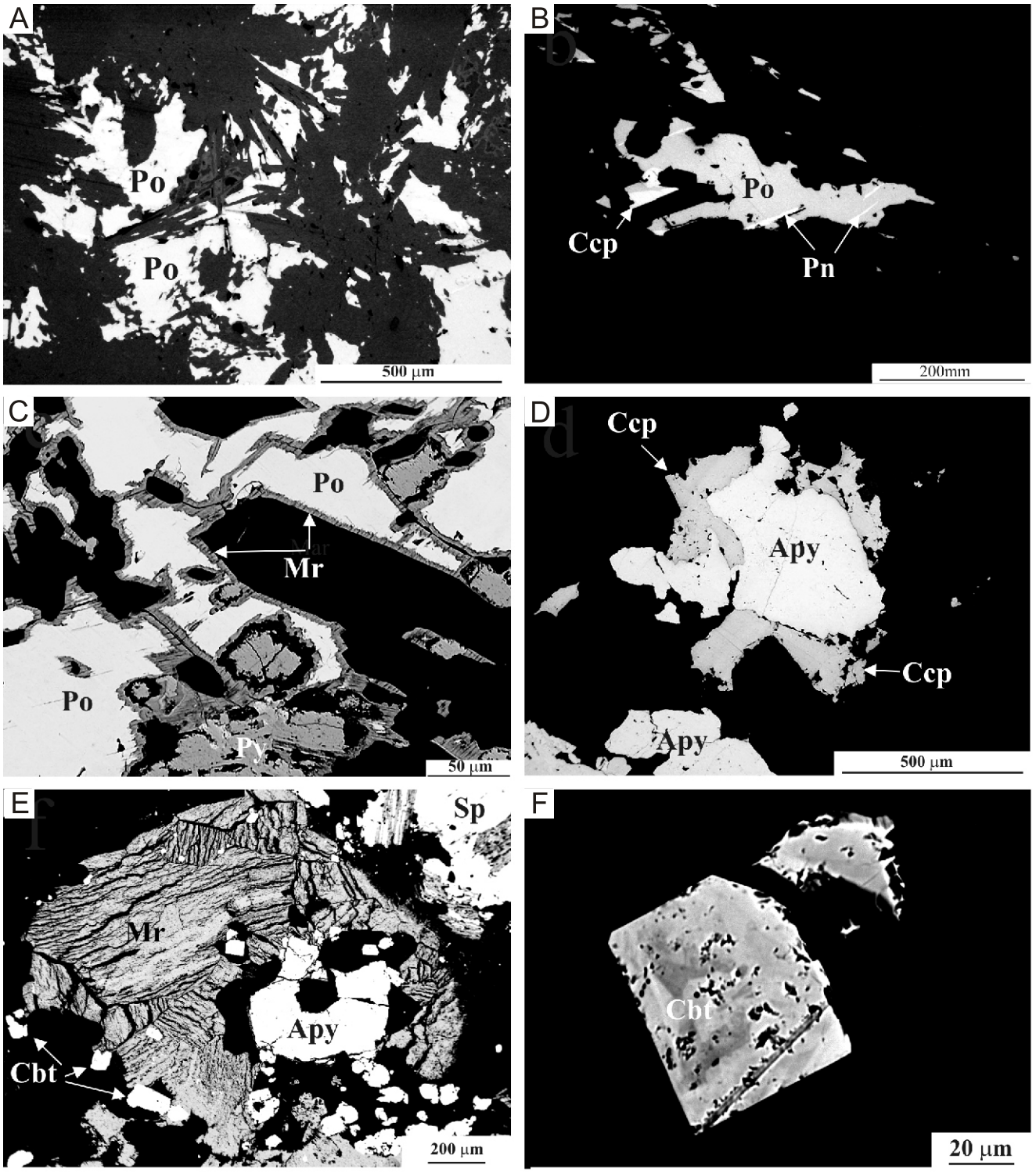

Fig. 7. BSE and microscopic images of ore minerals from the Budniki site

A — accumulation of pyrrhotite (Po) grains intergrown and partly replacing rock-forming minerals, sample Bud B, reflected light; **B** — aggregates of pyrrhotite (Po) intergrown with chalcopyrite (Ccp) and lamellar pentlandite (Pn), sample Bud N2, reflected light; **C** — pyrrhotite aggregate (Po) with pyrite (Py) intergrowths; pyrrhotite is replaced along grain boundaries and cracks by a mixture of marcasite (Mr) and pyrite resulting from initial weathering processes, sample Bud B2, BSA image; **D** — hipidiomorphic crystals of arsenopyrite (Apy) replaced by chalcopyrite (Ccp), sample Bud A2, reflected light; **E** — aggregate of arsenopyrite (Apy) and marcasite (Mr) accompanied by small, idiomorphic crystals of cobaltite (Cbt); large sphalerite (Sp) grain with relics of marcasite is also visible, sample Bud 7a, BSE image; **F** — idiomorphic crystals of cobaltite (Cbt) showing inhomogeneous chemical composition, sample Bud 7a, BSE image; abbreviations: Apy — arsenopyrite, Cbt — cobaltite, Mr — marcasite, Pn — pentlandite, Sp — sphalerite, other explanations as in Figure 6

Table 4

Average chemical compositions and formulae of pentlandite and pyrrhotite from the Budniki site analyzed using an electron microprobe (in wt.%)

	Pentlandite			Pyrrhotite	
S	32.37	32.51	32.61	39.04	39.24
Sb	0.00	0.00	0.00	0.01	0.01
As	0.02	0.05	0.04	0.02	0.01
Fe	28.66	27.72	28.56	58.70	59.87
Cu	0.00	0.00	0.00	0.00	0.00
Ni	35.24	35.43	35.95	1.10	0.26
Co	2.56	3.13	1.84	0.07	0.00
Mn	0.00	0.00	0.00	0.01	0.00
Total	98.86	98.84	99.00	98.96	99.39
Number of ions					
S	7.852	7.913	7.923	1.000	1.000
Sb	0.000	0.000	0.000	0.000	0.000
As	0.002	0.005	0.004	0.000	0.000
Fe	3.991	3.874	3.984	0.863	0.876
Cu	0.000	0.000	0.000	0.000	0.000
Ni	4.671	4.711	4.773	0.015	0.004
Co	0.338	0.415	0.243	0.001	0.000
Mn	0.000	0.000	0.000	0.000	0.000
N_{FeS}				0.927	0.933

Both the single sphalerite crystals and the aggregates show variable chemical composition. Particularly Fe, which is the principal substitute for Zn in sphalerite (Table 5a–e), reveals differences in concentration: the highest Fe contents exceed 7 wt.%, which corresponds to 13.8 ±1.2 mol% FeS, whereas the lowest values are below 0.5 wt.%, corresponding to 0.4 ±0.2 mol% FeS. The Cd contents are usually about 0.45–0.55 wt.% but, values up to 1.1 wt.%. were found also (Table 5a–e).

MARCASITE

Marcasite occurs as micrometres-thick rims overgrowing some pyrrhotite crystals (Fig. 7C), as thin streaks growing along the cleavage planes within large pyrrhotite aggregates, and as irregular intergrowths with pyrrhotite.

Marcasite rims around pyrrhotite are enriched in Ni (about 0.3 wt.%).

GALENA

Galena was encountered in small amounts as intergrowths with sphalerite (Fig. 8C) and chalcopyrite, and as disseminated crystals. Chemical analyses did not reveal any significant trace elements (e.g., Ag, Se, As).

PENTLANDITE

Relatively rare pentlandite was found as small, flame-like exsolutions within pyrrhotite aggregates (Fig. 7B). Its composition (Table 4) reveals that the grains analyzed are members of solid solution formed by $(Fe_{4.5}Ni_{4.5})S_8$, $Ni_{3\pm x}S_2$ and Co_4S_3 (Kitakaze and Sugaki, 2004).

ARSENOPYRITE

Arsenopyrite forms isometric aggregates, up to several millimetres across, embedded within and scattered around quartz veinlets (Fig. 7D, E). Common are xenomorphic aggregates of arsenopyrite and Co-arsenopyrite whereas idiomorphic grains are rare. Arsenopyrite forms intergrowths with cobaltite, chalcopyrite (the latter fills cracks in and cements the arsenopyrite crystals; Fig. 7D) and sphalerite.

COBALTITE

The identification of cobaltite and glaucodote grains brings some problems due to their optical similarity and unequivocal chemical composition. Taking into account the higher activity of S than As during the crystallization of the ore assemblage from Budniki reflected by the absence of (Co, Ni, Fe)-arsenides, all Co-rich phases are classified here as cobaltite, particularly if they form idiomorphic crystals.

Cobaltite tends to form fine (about 30 micrometres across), idiomorphic crystals scattered within quartz grains of quartz-arsenopyrite veinlets cutting the amphibolite. Moreover, cobaltite commonly forms hipidiomorphic grains, over 100 μm across, coexisting with arsenopyrite and/or accompanying marcasite (Fig. 7E). This variety is described as cobaltite 1. Small, euhedral crystals, reaching at most 30 μm in size, and scattered within quartz and sphalerite, were determined as cobaltite 2.

Large grains of cobaltite 1 show poor zonation (Fig. 7F). A representative composition of the irregular internal zone was recalculated to atomic %: 41.0 at.% S, 25.4 at.% As, 17.3 at. % Co, 12.0 at.% Fe and 4.3 at.% Ni. This is distinguished as the cobaltite 1a variety. The succeeding outer zone contains (after recalculation): 37.6 at.% S, 28.7 at.% As, 21.2 at.% Co, 8.5 at.% Fe and 4.0 at.% Ni. This is the cobaltite 1b variety. The outermost rim has 34.9 at.% S, 31.5 at.% As, 18.7 at.% Co, 7.6 at.% Fe and 7.3 at.% Ni. This was described as the cobaltite 1c variety. It is clear that during the crystallization of cobaltite, the S/As ratio progressively decreased (Fig. 9).

GERSDORFFITE

Gersdorffite is a rare ore component and is disseminated within the amphibolites together with the Ti minerals and pyrrhotite. Only occasionally it was encountered as tiny inclusions in sphalerite hosted in quartz-arsenopyrite veinlets.

Sulphide/sulphoarsenide mineralization is entirely genetically linked to the second variety of amphibolite. With the respect to the domains distinguished within the amphibolites, this mineralization is hosted in domains B and C.

MINERAL SUCCESSION AND FORMATION CONDITIONS OF THE ORE ASSEMBLAGE FROM THE BUDNIKI SITE

The ore mineral succession (Table 6) was obtained from microscopic studies of both the polished and thin sections, taking into account textures of mineral assemblages and host-rocks,

Table 5

Average chemical compositions and formulae of sphalerite and chalcopyrite from the Budniki site analyzed using an electron microprobe (in wt.%)

	Sphalerite					Chalcopyrite		
	a	b	c	d	e	I	II	III
S	33.18	32.82	33.06	33.36	33.21	34.54	34.93	34.77
Mn	0.02	0.00	0.00	0.02	0.02	0.01	0.00	0.03
Fe	0.23	1.60	4.35	6.16	7.91	30.19	29.80	28.84
Cu	0.02	0.00	0.05	0.15	0.54	33.94	33.68	32.72
Zn	66.22	63.90	61.52	59.24	56.95	0.08	0.87	2.64
As	0.00	0.00	0.00	0.02	0.02	0.02	0.03	0.03
Se	0.00	0.00	0.00	0.00	0.00	0.00	0.00	0.00
Ag	0.00	0.00	0.00	0.00	0.00	0.00	0.00	0.00
Cd	0.55	1.11	0.54	0.46	0.50	0.00	0.00	0.00
In	0.02	0.01	0.01	0.00	0.00	0.00	0.00	0.00
Sn	0.03	0.01	0.00	0.00	0.01	0.00	0.02	0.00
Sb	0.00	0.00	0.00	0.03	0.02	0.00	0.00	0.00
Te	0.00	0.00	0.00	0.00	0.00	0.00	0.00	0.00
Pb	0.00	0.00	0.00	0.00	0.00	0.00	0.00	0.00
Bi	0.00	0.00	0.00	0.00	0.00	0.00	0.00	0.00
Hg	0.00	0.00	0.00	0.00	0.00	0.00	0.00	0.00
Total	100.27	99.44	99.54	99.44	99.17	98.77	99.33	99.03
Number of ions								
S	1.012	1.008	1.006	1.017	1.009	2.002	2.023	2.022
Mn	0.000	0.000	0.000	0.000	0.000	0.000	0.000	0.001
Fe	0.004	0.028	0.076	0.108	0.138	1.005	0.991	0.963
Cu	0.000	0.000	0.001	0.002	0.008	0.993	0.984	0.960
Zn	0.990	0.962	0.918	0.885	0.849	0.002	0.025	0.075
As	0.000	0.000	0.000	0.000	0.000	0.001	0.001	0.001
Se	0.000	0.000	0.000	0.000	0.000	0.000	0.000	0.000
Ag	0.000	0.000	0.000	0.000	0.000	0.000	0.000	0.000
Cd	0.005	0.010	0.005	0.004	0.004	0.000	0.000	0.000
In	0.000	0.000	0.000	0.000	0.000	0.000	0.000	0.000
Sn	0.000	0.000	0.000	0.000	0.000	0.000	0.000	0.000
Sb	0.000	0.000	0.000	0.000	0.000	0.000	0.000	0.000
Te	0.000	0.000	0.000	0.000	0.000	0.000	0.000	0.000
Pb	0.000	0.000	0.000	0.000	0.000	0.000	0.000	0.000
Bi	0.000	0.000	0.000	0.000	0.000	0.000	0.000	0.000
Hg	0.000	0.000	0.000	0.000	0.000	0.000	0.000	0.000
% ZnS	0.4 ±0.2	2.8 ±0.6	7.6 ±1.1	10.8 ±0.4	13.8 ±1.2			

intergrowths of ore and rock-forming minerals, and the chemical compositions of the main constituents of the ore assemblage.

The observations revealed that the oldest assemblage comprises disseminated ilmenite and titanite blasts elongated concordantly to the foliation of the first variety of amphibolite. This mineralization is assigned to the metamorphic remobilization of elements from the amphibolite protoliths represented by basic volcanics and tuffs. A younger generation of Ti minerals includes a complex succession of mutually replacing ilmenite, titanite and rutile, all hosted in the second variety of amphibolite and related to retrogression at the end of regional metamorphism, and to succeeding stages of contact metamorphism. Generally, the Ti minerals are older than the sulphide-sulphoarsenide assemblage.

Among the sulphide-sulphoarsenide assemblage, pyrrhotite seems to be the earliest mineral. Pyrrhotite grains commonly contain flame-like exsolutions of pentlandite, which also seems to be an early phase. The succession of the remaining sulphides and sulphoarsenides observed under the microscope appears to be unequivocal. Hence, crystallization temperatures obtained with arsenopyrite (580–440°C) and sphalerite (450–250°C) geothermometers were used as additional criteria. As arsenopyrite crystallized in equilibrium with pyrrhotite and, later on, with pyrite and pyrrhotite, it is reasonable to infer the roughly contemporaneous formation of these phases. Chalcopyrite follows arsenopyrite, pyrrhotite and pyrite in the mineral succession. The position of Fe-Ni-Co-As-S phases is doubtful. Again, our microscopic observations do not provide unambiguous evidence, however, we think that cobaltite and gersdorffite are contemporaneous and follow the formation of the arsenopyrite-pyrrhotite-pyrite assemblage. The lower-temperature assem-

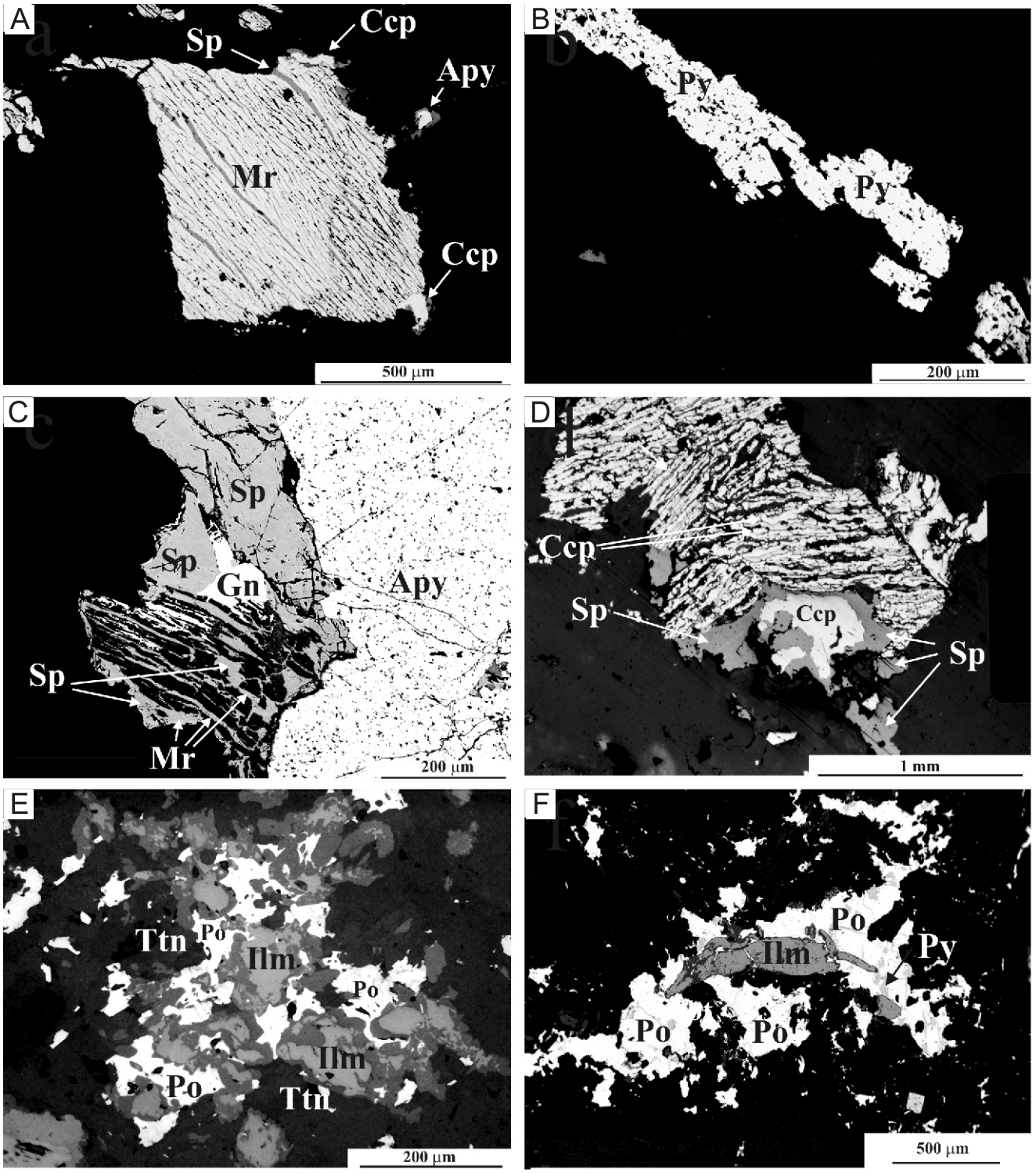

Fig. 8. BSE and microscopic images of ore minerals from the Budniki site

A — rib-like structure of marcasite aggregate (Mr) intergrown with sphalerite (Sp) and chalcopyrite (Ccp); small crystals of arsenopyrite (Apy) are also visible, sample Bud 6a, reflected light; **B** — accumulation of hipidiomorphic pyrite (Py) crystals arranged parallel to the foliation of the amphibolite, sample Bud 7, reflected light; **C** — relics of marcasite (Mr) replaced by (Sp) and galena (Gn) border a large arsenopyrite grain (Apy), sample Bud A (2), BSE image; **D** — marcasite (Mr) replaced by sphalerite (Sp) and chalcopyrite (Ccp), sample Bud 7a, reflected light; **E** — accumulation of ilmenite (Ilm) partly replaced by titanite and cemented by pyrrhotite (Po), sample Bud 4, reflected light; **F** — lensoid aggregate of ilmenite (Ilm) embedded within younger aggregate of xenomorphic pyrrhotite (Po) crystals with minute pyrite (Py) inclusions, sample Bud 8, BSE image; abbreviations: Gn — galena, other explanations as in Figures 6 and 7

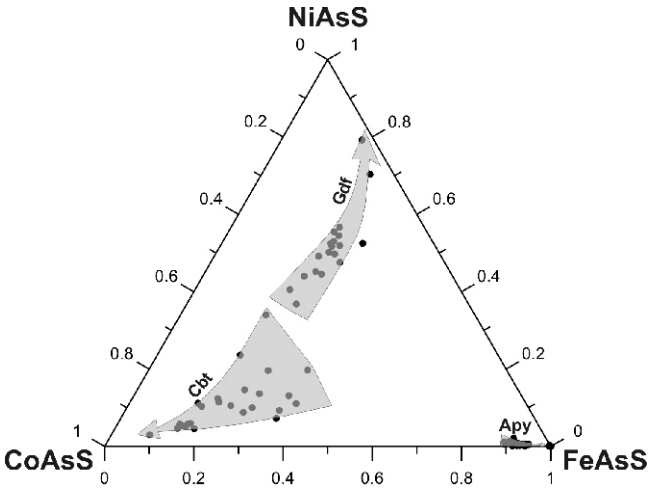

Fig. 9. Ternary plot of CoAsS-FeAsS-NiAsS system from Budniki (in atomic %)

Gdf — gersdorffite; grey arrows show compositional trends related to temperature decrease and progress of crystallization; other explanations as in Figure 7

blage comprises sphalerite and galena, with distinct evolution of the ZnS composition from high-Fe to low-Fe varieties.

Marcasite is observed as a late phase, rimming large, nest-like pyrrhotite aggregates and filling the cracks within these aggregates. Its formation is presumably related to the early stages of weathering at waste dumps. Trace amounts of covellite result from late transformations of chalcopyrite and may also be related to the initial weathering processes.

DISCUSSION

As shown earlier, the crystallization of ilmenite and part of the titanite was connected mainly with the regional metamorphism during which the products of Early Palaeozoic bimodal volcanism were metamorphosed under amphibolite facies conditions (550–600°C, p ~ 6 kbar) and transformed into amphibolites. Major and trace element analyses of the Budniki amphibolite (B2) indicate an alkali basalt character and within-plate-type tectonic emplacement setting of its protolith (Oberc-Dziedzic *et al.,* in press.). Although the Ti content in the Budniki amphibolite is higher (4.4 wt.%) than those in typical within-plate basalts (3.09–2.11 wt.%; Wilson, 1993) and in other alkali metabasalts from the southeastern part of the Izera–Kowary Unit (3.7–3.25 wt.%; Winchester *et al*., 1995),

Table 6

Ore mineral succession of the Budniki site (uranium mineralization data after Kaczmarek, 1959)

Mineral	Stages				
	Protolith	Regional metamorphism 600–550°C 6 kbar	Contact metamorphism		Weathering
Ilmenite	==========	I ==========		II ======?	
Titanite	——-----?-----	I ==========	II ==========	=====	
Rutile			I =====	I II ==== ==== (II) 625	
Pyrrhotite		?======?		I (625?) II (560–510) ======= =======	
Wolframite, scheelite				?======?	
Pentlandite				(625) =======	
Gersdorffite				(600?) =======	
Arsenopyrite				(580–440) ========	
Cobaltite				(500?) ========	
Pyrite				?==========?	
Chalcopyrite		? ===?		I II (440–370) ======= =======	
Sphalerite				(450–250) = ======	
Galena				=======	
Marcasite				?====?	?=========
Covellite					————
Uranium minerals				?==========?	==========

such features as the arrangement of ilmenite grains parallel to the foliation, and the lack of evidence for crystallization of ilmenite from external sources, suggest that Ti should be derived from the protolith of the amphibolites. The source of Ti for Al-titanite and rutile might have been ilmenite and tschermakite.

During the contact metamorphism caused by the Karkonosze intrusion, which evolved from retrogression (540°C) to peak temperatures (635°C) and then, again to retrogression (470°C) Ti mineralization was subjected to intensive alteration, as indicated by the replacement of ilmenite by Al-rich titanite, ilmenite by rutile, and the crystallization of large rutile grains. High-temperature fluids derived from the intrusion, carrying both S and As (with S dominating over As) resulted in the crystallization of an ore assemblage composed of sulphides and sulphoarsenides.

Thermochemical conditions of ore mineral formation were determined based on the compositions of pyrrhotite, arsenopyrite and sphalerite, taking into account textural relationships between these minerals and the coexisting phases. The compositions of arsenopyrite crystals were drawn onto the sulphur fugacity (log fS_2) *vs.* temperature (T) diagram for the Fe-As-S system (see Kretschmar and Scott, 1976, modified by Sharp *et al*., 1985; Fig. 10). Limitations of the arsenopyrite geothermometer, resulting from the common inhomogenity of the arsenopyrite crystals (Kerestedjian, 1997), were taken into account. Following Sharp *et al*. (1985), the impact of pressure on arsenopyrite composition buffered by pyrrhotite and pyrite in low-pressure hydrothermal deposits is insignificant and here it has been ignored. Additionally, N_{FeS} isopleths of the FeS mole fraction in the FeS-S_2 system (Toulmin and Barton, 1964) and concentration lines of FeS content (mole %) in sphalerite (Barton and Toulmin, 1966; Scott, 1983) were marked in the Fe-As-S diagram.

Our data suggest that the ore minerals crystallized successively from hot, hydrothermal fluids of complex Fe-Ni-Co-Cu-Zn-S-As composition, starting from Ni-enriched pyrrhotite, (Fe, Ni)-enriched cobaltite, Co-arsenopyrite and Co-free arsenopyrite. Exsolutions of pentlandite within some pyrrhotite grains coexisting with chalcopyrite and, on the other hand, the crystallization of (Co, Fe)-sulphoarsenides only in quartz veins cutting both the amphibolite and the adjacent quartzofeldspathic schists, indicate that sulphur fugacity strongly predominated over that of arsenic at the beginning of the mineralization process. Pentlandite is a phase unknown in the (Fe-Co-Ni)-As-S system, and Ni clearly concentrates in the monosulphide solid solution (*mss*) corresponding to pyrrhotite with a high S/As ratio (Hem and Makovicky, 2001). According to many authors (e.g. Kullerud, 1963; Vaasjoki *et al*., 1974; Kaneda *et al.*, 1986; Vaughan and Craig, 1997), pentlandite in the Fe-Co-Ni-S system forms at temperatures below 610°C. Kullerud (1963) showed even a correlation between the Co content of pentlandite and the temperature of its formation. However, Sugaki and Kitakaze (1998) and Kitakaze and Sugaki (2004) proved that pentlandite of composition close to $Fe_{4.5}Ni_{4.5}S_8$ does not break at a temperature of 615 ±3°C, but inverts to a high-temperature form stable up to 865 ±3°C. Taking into account these data, the pyrrhotite-pentlandite assemblage found in the Budniki site could be the product of decomposition of a higher-temperature *mss,* enriched in Ni. This phase exsolved into pentlandite and residual *mss* (pyrrhotite) with lower Ni content. The representative composition of such high-temperature pyrrhotite can be close to those grains which reveal the highest Ni and Co contents, and are associated either with exsolutions or with separate grains of pentlandite. Taking into account the Co-T correlation after Kullerud (1963), the exsolution temperature of pentlandite from high-temperature *mss* can be estimated as about 625°C. The temperature of pyrrhotite crystallization can be estimated based on the composition of pyrrhotite in FeS-S_2 system (Toulmin and Barton, 1964) but, unfortunately, the pyrrhotite from Budniki commonly contains significant amounts of Ni and traces of Co. Therefore, the fraction N_{FeS} = 0.930(4) was obtained only for the grains lowest in Ni (about 0.4 wt.%). This value of N_{FeS} indicates the crystallization of pyrrhotite close to the Py/Po-equilibrium at temperatures of about 510–560°C (Fig. 10). Pyrrhotite containing higher amounts of Ni probably crystallized at higher temperatures, corresponding even to those at which pentlandite exsolved.

Phase relationships in the (Fe, Co, Ni)$As_{0.5}S_{1.5}$ system at 650 and 500°C have recently been investigated by Hem and Makovicky (2004). According to these authors, Fe-rich cobaltite coexists with the *mss* and $As_{1-x}S_x$ melt at 650°C, and it crystallizes together with arsenopyrite and pyrite at 500°C. Furthermore, the *mss* (Fe, Co, Ni)$_{1-x}$S, is always formed in Fe-bearing systems, and at 650°C it contains up to 0.2 at.% As, along with variable amounts of (Fe, Co, Ni), ranging between 45.5–47.4 at.% (Fe + Co + Ni). At 500°C, the *mss* contains up to 0.7 at.% As, <3.7 at.% Co and variable amounts of Fe and Ni. Cobaltite, which crystallizes at 650°C, contains <10.8 at.% Fe, but at 500°C this phase reveals up to 4 at.% Fe and <7.9 at.% Ni. Pentlandite was not observed in the system investigated (Hem and Makovicky, 2004).

We suggest that in the Budniki mineralization the following phases crystallized successively from the (Fe-Co-Ni-As-S)-fluids: (Fe, Co) gersdorffite, (Fe, Ni) cobaltite and Co arsenopyrite of composition close to (Fe, Co)AsS. These were followed by gersdorffite, cobaltite and arsenopyrite relatively low in Co and Ni (Fig. 9). Gersdorffite crystallized only in the form of small, disseminated grains within amphibolite, but it is almost absent from all other forms of ore mineralization at the Budniki site, especially from the quartz-arsenopyrite veinlets containing Co-rich mineralization. Therefore, it seems to be a product of reaction between the amphibolite and the fluids. The crystallization of gersdorffite and (Fe, Ni) cobaltite might have taken place at temperatures close even to 600°C. According to Hem and Makovicky (2004), at this temperature the *mss* becomes more and more enriched in Fe, and more depleted in both Co and Ni. At the final stage of arsenopyrite crystallization (Co, Ni)-free arsenopyrite can crystallize, according to the reaction: $FeS_{(pyrrhotite)} + As_{(lq)} = FeAsS$ and $FeS_{2(pyrite)} + As_{(lq)} = FeAsS$. The temperature and sulphur fugacity $f(S_2)$ during this crystallization process has been estimated using the arsenopyrite geothermometer (Toulmin and Barton, 1964; Sharp *et al*., 1985). For the observed As content in the Co-low arsenopyrite (ranging from 35.1 to 32.4 at.%) it can be assumed that crystallization was first buffered by pyrrhotite at 580°C, than also by pyrite at about 440°C. The sulphur fugacity expressed as

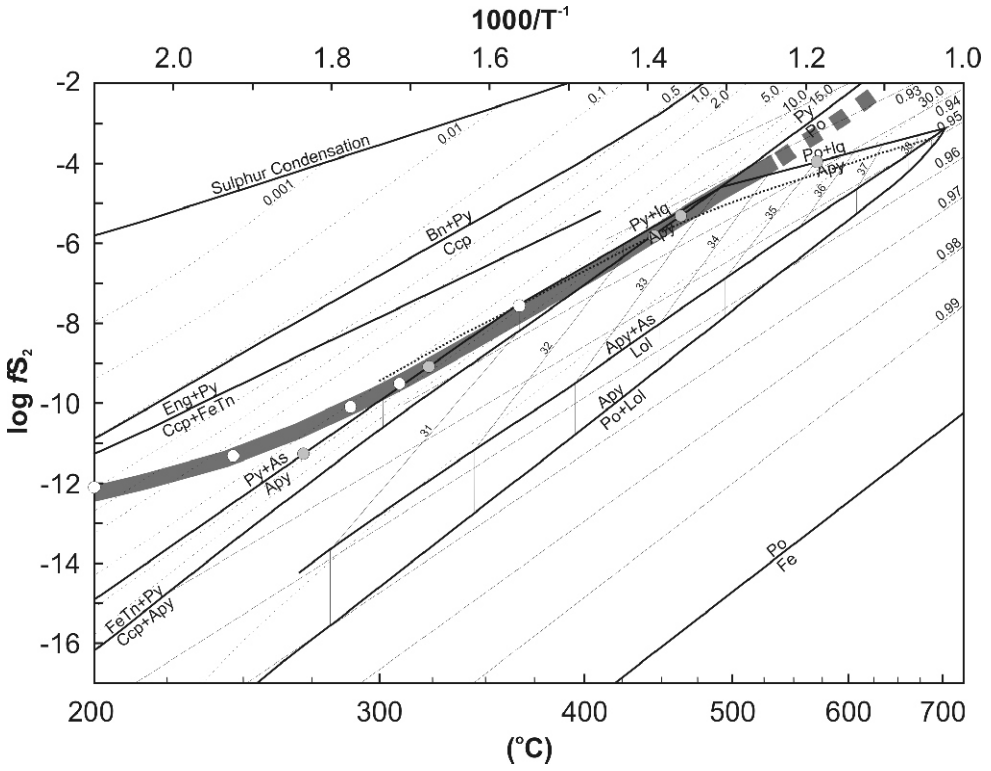

Fig. 10. Patch of physical-chemical evolution (heavy line) of crystallization environment of pyrrhotite-arsenopyrite-sphalerite assemblage from the Budniki camp in the sulphur fugacity (log $f S_2$) *vs* temperature (T) diagram (after Toulmin and Barton, 1964, Barton and Toulmin, 1966; Kretschmar and Scott, 1976; Sharp *et al*., 1985; Scott, 1983)

log$f(S_2)$ varied in time from about –4 to about –6. The (Fe, Ni) cobaltite was commonly observed inside the Co-low arsenopyrite grains. It had to crystallize after the exsolution of pentlandite, possibly together with pyrrhotite, at a slightly higher temperature than that determined for arsenopyrite. During the crystallization of gersdorffite, cobaltite and arsenopyrite, the contents of Fe and Ni in these minerals progressively decreased and the final, (Fe, Ni)-low cobaltite could crystallize at temperatures below 500°C (Fig. 10), as for Co-free arsenopyrite.

Chalcopyrite forms intergrowths with pyrrhotite, arsenopyrite, pyrite and sphalerite, which suggests a wide range of crystallization temperatures. In the Budniki mineralization sphalerite very often occurs as large, polymineral aggregates in which it replaces and coalesces all the earlier phases. Sphalerite grains are inhomogeneous in composition. During its continuous crystallization, the Fe content progressively decreased, from about 13.8 to about 0.4 mol% FeS. Based on the FeS content in sphalerite quoted by Scott (1983), the temperatures of ZnS crystallization can be estimated as 450°C for the early phases, down to about 250°C for the late ones (Fig. 10).

Correspondingly, sulphur fugacity varied from –7 to about –10. Many sphalerite crystals show numerous inclusions, particularly of chalcopyrite. Intergrowths of sphalerite with chalcopyrite and less commonly with galena were also observed. Chalcopyrite inclusions within sphalerite contains as much as 2.6 wt.% Zn. The temperature of such exsolutions was estimated at 440–370°C (Scott, 1983; Fig. 10).

A conceptual model of the Budniki mineralization (Table 7) includes the following stages: Early Ordovician bimodal volcanism and Early Ordovician intrusion of the Kowary Gneiss protolith succeeded by Early Variscan regional metamorphism and, finally, followed by Variscan magmatism (the Karkonosze Granite intrusion), and related contact metamorphism accompanied by hydrothermal activity.

In such a scheme, the bulk of Ti mineralization is related to both the regional and contact metamorphism. The source of Ti could be the protolith of the amphibolites. By contrast, the bulk of the Fe-Ni-Co-Cu-Zn-Pb sulphide and arsenide mineralization is clearly linked to the contact metamorphism and related hydrothermal activity of the Karkonosze Granite. The intrusion was, most likely, the source of both the thermal energy and the elements, except for a part of the Fe, which might have come from transformation of amphiboles and ilmenite. One can assume that the early stage of mineralization (high-temperature pyrrhotite with pentlandite exsolutions, arsenopyrite) could have been related to the second episode of contact metamorphism represented by the Mg-hornblende II/Ca-plagioclase/clinopyroxene assemblage (temperatures 622–635°C). The replacement of radiating amphibole crystals by pyrrhotite may be a sign of this process. The further mineralization stages took place during the third episode of contact metamorphism (temperatures 473–511°C) connected with shearing, which apparently facilitated the circulation of hydrothermal fluids. This is supported by the presence of ore minerals within and around the quartz-feldspar veinlets.

Table 7

Model of ore mineralization in the Budniki site related to geological processes

MAGMATISM AND METAMORPHISM	TRANSFORMATION OF COUNTRY ROCKS	Ti MINERALS IN AMPHIBOLITE	ORE MINERALS	TEMPERATURE (°C)
VARISCAN MAGMATISM KARKONOSZE GRANITE (Contact metamorphism; Hydrothermal processes)	amphibolite II	Al-titanite ilmenite exsolutions in rutile rutile (large crystals) ilmenite→rutile (needle) ilmenite→Al-titanite	U-minerals* sphalerite chalcopyrite I, II cobaltite arsenopyrite gersdorffite pentlandite pyrrhotite I, II	450–250 440–370 500? 580–440 <600 600? 625 635–620 ? 540
EARLY VARISCAN REGIONAL METAMORPHISM	Kowary gneiss; amphibolite I; quartzofelds patic rocks	ilmenite-rutile intergrowths ilmenite, titanite traces of pyrrhotite		600–550
EARLY ORDOVICIAN BIMODAL MAGMATISM	granite; basic volcanic and volcanoclastic rocks; acidic volcano-clastic rocks	Ti-bearing rock-forming minerals ilmenite		

Based on the ore mineral succession, we suggest that hydrothermal solutions evolved from high-temperature, high S/high Fe, to high As/high Ni/Co, then to high Zn fluids. Because Cu, Ni, Co, Zn, Pb and As do not occur in large quantities in the host amphibolites, a magmatic origin for the hydrothermal solutions is probable.

In conclusion, the Budniki mineralization belongs to the Variscan ore-forming episode related to the activity of the Karkonosze Granite. Considering the mineralization stages in the eastern envelope of the Karkonosze Granite distinguished by Mochnacka (2000), the Budniki mineralization can be correlated with the transition from stages II to III. Stage II was proposed to represent the high-temperature mineralization in the contact zone of the granite whereas stage III was a typical vein-type hydrothermal mineralization, also related to the granite activity.

CONCLUSIONS

Based on microscopic observations and chemical analyses, the following characteristics of the ore-forming processes can be formulated:

1. The Budniki Ti-oxide/Fe-Cu-Ni-Co-Zn-Pb-sulphide-sulphoarsenide mineralization, although uneconomic, provides an interesting contribution to the understanding of the relationships between metamorphism, hydrothermal processes and ore mineralization related to the activity of the Variscan Karkonosze Granite intrusion.

2. Ore mineralization is hosted in amphibolites and, much less significantly, in quartzofeldspathic schists.

3. The source of Ti is interpreted to be the protolith of the amphibolites. Ti mineralization includes the ilmenite-titanite assemblage formed during regional metamorphism, followed by decomposition of ilmenite and crystallization of Al-titanite and rutile during contact metamorphism.

4. Polymetallic sulphide-sulphoarsenide mineralization includes: pyrrhotite, pyrite, chalcopyrite, arsenopyrite, gersdorffite, cobaltite, sphalerite, galena and marcasite precipitated during contact metamorphism from hydrothermal solutions, at a temperature range from 625°C (based on pyrrhotite-pentlandite intergrowths) through 580–440°C (arsenopyrite geothermometer) to 450–250°C (sphalerite geothermometer).

5. Hydrothermal solutions were of magmatic origin, as the hosting amphibolites do not contain significant amounts of metals (except iron) to be leached and deposited as a sulphide-sulphoarsenide assemblage.

6. The Budniki mineralization belongs to the Variscan ore-forming episode related to the activity of the Karkonosze Granite and is correlated with the early stage of polymetallic mineralization, which culminated in the formation the well-known Kowary and Miedzianka polymetallic deposits, both intensely mined in the past.

Acknowledgements. Sincere thanks are due to Prof. R. Kryza from University of Wrocław for kind assistance and helpful discussion. Prof. R. Klemd and an anonymous reviewer are thanked for their constructive reviews. The kind help of Dr. P. Dzierżanowski and Ms. L. Jeżak from the University of Warsaw in carrying out the microprobe analyses is also very much appreciated. The research project was financed by the Polish Committee of Scientific Research, grant No. 5 T12B 036 25.

REFERENCES

BARTON P. B. and TOULMIN P. (1966) — Phase relationships involving sphalerite in the Fe-Zn-s system. Econ. Geol., **61**: 815–848.

BORUCKI J., GŁOWACKI Z., MASŁOWSKI W., SAŁDAN M., UBERNA J. and ZAJĄCZKOWSKI W. (1967) — Ocena perspektyw poszukiwawczych złóż uranu w Polsce. Wyd. Geol. Warszawa.

BUCHER K. and FREY M. (1994) — Petrogenesis of metamorphic rocks. Springer Verlag.

CHALOUPSKÝ J. ed. (1989) — Geology of the Krkonoše and Jizerské hory Mts. (in Czech with English summary). Ustřední Ústav Geol. Praha.

DUTHOU J.-L., COUTURIE J.-P, MIERZEJEWSKI M. P. and PIN C. (1991) — Next dating of granite sample from the Karkonosze Mountains using Rb-Sr total rock isochrone method (in Polish with English summary). Prz. Geol., **36** (2): 75–79.

HARLOV D., TROPPER P., SEIFERT W., NIJLAND T. and FÖRSTER H. J. (2006) — Formation of Al-rich titanite ($CaTiSiO_4O$–$CaAlSiO_4OH$) reaction rims on ilmenite in metamorphic rocks as a function of fH_2O and fO_2. Lithos, **88**: 72–84.

HEM S. R. and MAKOVICKY E. (2001) — Compositional trends in Fe, Co and Ni sulfarsenides and their crystals — chemical implications: results from the Arroyo de la Cueva deposits, Ronda Peridotite, Southern Spain. Can. Miner., **39**: 831–853.

HEM S. R. and MAKOVICKY E. (2004) — The system Fe-Co-Ni-As-S. I. Phase relations in the (Fe, Co, Ni)$As_{0.5}S_{1.5}$ section at 650° and 500°C. Can. Miner., **42**: 43–62.

HOLLAND T. and BLUNDY J. (1994) — Non-ideal interactions in calcic amphiboles and their bearing on amphibole-plagioclase thermometry. Contrib. Miner. Petrol., **116**: 433–447.

JOHN T., KLEMD R., HIRDES W. and LOH G. (1999) — The metamorphic evolution of the Palaeoproterozoic (Birimian) volcanic Ashanti belt (Ghana, West Africa). Precambrian Research, **98**: 11–30.

KANEDA H., TAKENOUCHI S. and SHOJI T. (1986) — Stability of pentlandite in the Fe-Ni-Co-S system. Miner. Deposita, **21**: 169–180.

KACZMAREK L. (1959) — Uranium exploration report (unpublished data) (in Polish). Arch. R-1 Company.

KERESTEDJIAN T. (1997) — Chemical and morphological features of arsenopyrite, concerning its use as a geothermometer. Miner. Petr., **60**: 231–243.

KITAKAZE A. and SUGAKI A. (2004) — The phase relationships between $Fe_{4.5}Ni_{4.5}S_8$ and Co_9S_8 in the system Fe-Ni-Co-S at temperatures from 400° to 1100°C. Can. Miner., **42**: 17–42.

KRETSCHMAR U. and SCOTT S. D. (1976) — Phase relations involving arsenopyrite in the system Fe-As-S and their application. Can. Miner., **14**: 364–386.

KULLERUD G. (1963) — Thermal stability of pentlandite. Can. Miner., **8**: 353–366.

LEAKE B., WOOLEY A. R., ARPS C. E. S., BIRCH W. D. *et al*. (1997) — Nomenclature of amphiboles: report of the Subcommittee on Amphiboles of the International Mineralogical Association, Commission on New Minerals and Mineral Names. Can. Miner., **35**: 219–246.

MASSONNE H. J. and SCHREYER W. (1987) — Phengite geobarometry based on the limiting assemblage with K-feldspar, phlogopite, and quartz. Contrib. Mineral. Petrol., **96**: 112–224.

MAZUR S. (1995) — Structural and metamorphic evolution of the country rocks at the eastern contact of the Karkonosze Granite in the southern Rudawy Janowickie Mts. and Lasocki Range (in Polish with English summary). Geol. Sudet., **29**: 31–98.

MAZUR S. and ALEKSANDROWSKI P. (2001) — The Tepla(?)/Saxothuringian suture in the Karkonosze-Izera Massif, Western Sudetes, Central European Variscides. Internat. J. Earth Sc., **90**: 341–360.

MIERZEJEWSKI M. P. and OBERC-DZIEDZIC T. (1990) — The Izera-Karkonosze Block and its tectonic development (Sudetes, Poland). Neues Jahrb. Geol. Paläont. Abh., **179**: 197–222.

MIYASHIRO A. (1994) — Metamorphic Petrology. UCL Press.

MOCHNACKA K. (2000) — Prawidłowości wykształcenia mineralizacji kruszcowej w metamorficznej osłonie granitu Karkonoszy — próba powiązania ze środowiskiem geotektonicznym. Miner. Soc. Poland, Spec. Pap., **16**: 223–258.

MOCHNACKA K. and BANAŚ M. (2000) — Occurrence and genetic relationships of uranium and thorium mineralization in the Karkonosze-Izera Block (the Sudety Mts., SW Poland). Ann. Soc. Geol. Pol., **70**: 137–150.

MOCHNACKA K., OBERC-DZIEDZIC T., MAYER W., PIECZKA A. and GÓRALSKI M. (2007) — Occurrence of sulphides in Sowia Dolina near Karpacz (Sw Poland) — an example of ore mineralization in the contact aureole of the Karkonosze granite — Poland. Miner. Pol., **38** (2): 185–207.

NASIR S. and OKRUSCH M. (1997) — Metabasites from the central Vor-Spessart, norh-west Bavaria. 2. Comparison of different geothermometers and geobarometers. Chemie der Erde-geochemistry, **57**: 25–50.

OBERC-DZIEDZIC T. (2003) — The Izera granites: an attempt of the reconstruction of predeformational history (in Polish with English summary). In: Sudety Zachodnie: od wendu do czwartorzędu (eds. W. Ciężkowski, J. Wojewoda and A. Żelaźniewicz): 41–52. WIND Wrocław.

OBERC-DZIEDZIC T., KRYZA R., MOCHNACKA K. and LARIONOV A. (in press) — Ordovician passive continental margin magmatism in the Central-European Variscides: U-Pb zircon data from the SE part of the Karkonosze-Izera Massif, Sudetes, SW Poland. Internat. J. Earth Sc., DOI: 10.1007/s00531-008-0382-4.

PLYUSNINA L. P. (1982) — Geothermometry and Geobarometry of plagioclase-hornblende bearing assemblages. Contrib. Miner. Petrol., **80**: 140–146.

RAMDOHR P. (1969) — The ore minerals and their intergrowths. Pergamon Press.

ROBINSON P., SPEAR F. S., SCHUMACHER J. C., LAIRD J., KLEIN C., EVANS B. W. and DOOLAN B. L. (1982) — Phase relations of metamorphic amphiboles: natural occurrence and theory. In: Amphiboles and Other Hydrous Pyriboles — Mineralogy (eds. D. R. Veblen and P. H. Ribbe). Rev. Miner., **9B**.

RÓŻAŃSKI P. (1995) — Zdjęcie geologiczne głównego grzbietu Karkonoszy między Czołem a Czarnym Grzbietem. Mcs. Thesis. Archiv. Univ. Wroc.

SCOTT S. D. (1983) — Chemical behaviour of sphalerite and arsenopyrite in hydrothermal and metamorphic environments. Miner. Mag., **47**: 427–435.

SHARP Z. D., ESSENE E. J. and KELLY W. C. (1985) — Reexamination of the arsenopyrite geothermometer: pressure considerations and applications to natural assemblages. Can. Miner., **23**: 517–534.

SUGAKI A. and KITAKAZE A. (1998) — High form of pentlandite and its thermal stability. Am. Miner., **83**: 133–140.

TOULMIN P. and BARTON P. B. (1964) — A thermodynamic study of pyrite and pyrrhotite. Geochim. Cosmochim. Acta, **28**: 641–671.

VAASJOKI O., HAEKLI A. and TONTTI M. (1974) — The effect of cobalt on the thermal stability of pentlandite. Econ. Geol., **69**: 549–551

VAUGHAN D. J. and CRAIG J. R. (1997) — Sulfide ore mineral stabilities, morphologies, and intergrown textures. In: Geochemistry of Hydrothermal Ore Deposits (ed. H. L. J. Barnes). Wiley and Sons, Inc., New York.

VERNON R. H. (2004) — A practical guide to rock microstructure. Cambridge University Press.

WILSON M. (1993) — Igneous Petrogenesis. Harper Collins Academic.

WINCHESTER J. A., FLOYD P. A., CHOCYK M., HORBOWY K. and KOZDRÓJ W. (1995) — Geochemistry and tectonic environment of Ordovician meta-igneous rocks in the Rudawy Janowickie Complex, SW Poland. J. Geol. Soc. London, **152**: 105–115.